Computers and Geotechnics 163 (2023) 105759

Contents lists available at ScienceDirect

Computers and Geotechnics

journal homepage: www.elsevier.com/locate/compgeo

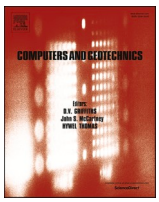

Revisiting Active and Passive Earth Pressure Problems using Three Stability Factors

Tan Nguyen [a,b], Jim Shiau [c,*]

[a] Smart Computing in Civil Engineering Research Group, Ton Duc Thang University, Ho Chi Minh City, Viet Nam
[b] Faculty of Civil Engineering, Ton Duc Thang University, Ho Chi Minh City, Viet Nam
[c] School of Engineering, University of Southern Queensland, Toowoomba, QLD, 4350, Australia

ARTICLE INFO

Keywords:
Earth Pressure Factors
Retaining Walls
Finite Element Limit Analysis

ABSTRACT

This paper presents rigorous plasticity solutions to the classical active and passive earth pressure problems. The primary method adopted is a conventional equation based on the soil property and three stability factors (F_c, F_s, and F_γ), that are analogous to Terzaghi's bearing capacity factors (N_c, N_s, and N_γ) of strip footings. The proposed method is considered as a practical yet smart approach to the determination of earth pressures and is one of the main novelties in this study. To achieve this, the finite element limit analysis (FELA) of upper and lower bounds solutions, a powerful tool in studying the behaviour of soil stability, is employed to compute the three stability factors for a wide range of soil internal friction angles, wall roughness, and surcharge pressures. In addition, analytical solutions based on statistically admissible stress fields are adopted to validate the proposed FELA solutions. The validation satisfactorily demonstrated the accuracy and reliability of the proposed solutions. It follows that the numerical results are presented in the form of tables, figures, and several examples provided to demonstrate the practical use of the three factors in estimating active and passive earth pressures with various backfill soils, wall roughness, and surcharge pressure. The study should, therefore, be of value to practitioners.

1. Introduction

Determination of active and passive earth pressures is a routine process in the design of soil structures such as retaining walls and bridge abutments. Factors that influence the magnitude of the lateral earth pressures have been reported by Duncan and Mokwa (2001). For rigid retaining structures, soil property (cohesion and internal friction angle), mode of wall movement, soil-wall roughness, and wall shape are considered the most influential parameters.

Traditionally, the design of retaining structures was executed by using the limit equilibrium method where the earth pressures acting on the wall are derived from the classical earth pressure theories i.e., Rankine or Coulomb. Both the active and passive earth pressures are characterized by the active earth pressure coefficient (K_a) and the passive earth pressure coefficient (K_p), which are dependent on the internal friction angle of backfill soil (ϕ), the friction angle of the soil-wall interface (δ), the slope of the backfill and the wall geometry. In Rankine's earth pressure theory, the retaining wall is assumed to be smooth whereas Coulomb's theory considers the soil-wall friction. Many researchers have since studied the earth pressure problems using various methods such as the limit equilibrium method, the method of stress characteristics, and the limit analysis method.

With regards to the limit equilibrium method, Terzaghi (1943) and Terzaghi (1967) proposed various failure mechanisms to determine the minimum earth pressure exerted by cohesionless soil. Caquot and Kerisel (1948) used a log spiral mechanism to study the variation of the passive earth pressure coefficient.

Shields and Tolunay (1973), Basudhar and Madhav (1980) used the method of slices to calculate the coefficient of passive pressure for cohesionless backfill soils. A study of passive earth pressure using triangular slices based on the state of limit equilibrium was conducted by Zhu and Qian (2000). Recently, Liu et al. (2018) proposed a modified logarithmic spiral method to figure out the passive earth pressure. It's important to highlight that the stress equilibrium condition has been disregarded due to the application of the limit equilibrium method ~ an upper-bound type approach that carries the potential for errors, as emphasized by Nguyen (2022, 2023a).

Numerous researchers have demonstrated that the distribution of active and passive earth pressures on a retaining wall is non-linear for walls with rough interfaces (Tsagareli 1965, Fang and Ishibash 1986, Chang 1997, O'Neal and Hagerty 2011). As stated by Iskandern et al.

* Corresponding author.
E-mail addresses: nguyentan@tdtu.edu.vn (T. Nguyen), jim.shiau@usq.edu.au (J. Shiau).

https://doi.org/10.1016/j.compgeo.2023.105759
Received 21 March 2023; Received in revised form 22 August 2023; Accepted 25 August 2023
Available online 31 August 2023

Nomenclature

H (unit in meter) Height of the retaining wall
x, z Coordinates in a rectangular coordinate system (xOz)
r,θ Radial and angular coordinates in a polar coordinate system (r,θ)
σ_x, σ_z, τ_{xz} Components of horizontal, vertical, and shear stress in rectangular coordinates (xOz) (compression taken as positive)
σ_r, σ_θ, $\tau_{r\theta}$ Components of radial, angular, and shear stress in polar coordinates (r, θ) (compression taken as positive)
σ_s (unit in kPa) surcharge load;
p In-plane mean stress, $p = (\sigma_r + \sigma_\theta)/2$
F_c, F_s, F_γ Factors for active and passive earth pressure due to cohesion (F_c), surcharge loading (F_s), and soil weight (F_γ)
γ (unit in kN/m^3) Unit weight of the backfill soil (assumed uniform and constant throughout the retaining wall backfill)
ϕ (unit in degree) The internal friction angle of the backfill (value in design);
χ Non-dimensional mean stress;
ψ (unit in degree) Relative angle of the major principal stress made by the direction of major principal stress with the radial direction (positive sign for counterclockwise direction);
ψ_w (unit in degree) Relative angle of the major principal stress on the wall rear face ($\theta = 0$)
Ψ (unit in degree) Angle of the major principal stress made by the direction of major principal stress with the gravitational direction (positive sign for counterclockwise direction)
p_a and p_p (unit in kPa) Active and passive earth pressures
P_a and P_p (unit in kN/m) Total active and passive thrusts
R wall roughness;
δ (unit in degree) the interface frictional angle
c_{int} (unit in kPa) the interface cohesion
c (unit in kPa) the effective cohesion.

(2013), this non-linearity substantially depends on the friction angle of the soil-wall interface and modes of wall movement as well. Patki et al. (2017) have recently developed a numerical protocol using Kotter's equation for estimating coefficients of passive earth pressure on an inclined rigid retaining wall with the assumption of a log-spiral failure surface.

Using the method of stress characteristics, Kumar and Chitikela (2002) obtained coefficients of passive earth pressure for an inclined retaining wall with non-cohesive backfill under horizontal pseudo-static seismic forces. Elasto-plastic analysis for the classical passive earth pressure problems was studied by Shiau and Smith (2006) using the explicit finite difference method. Shiau and Smith (2006) examined a wide range of factors, including the effect of friction on the soil wall interface as well as the effects of boundary conditions and the associated and non-associated flow rule. Benmeddour et al. (2012) produced the coefficients of active and passive earth pressures for rigid retaining walls with multiple geometrical and mechanical backfill configurations using the explicit finite difference method.

Finite Element Limit Analysis (FELA) has revolutionized the understanding of lateral earth pressure complexities, notably in retaining wall scenarios. This method's prowess is evidenced by pivotal studies showcasing its adaptability. Chen and Rosenfarb (1973) applied the upper bound theorem to quantify active and passive earth pressures in cohesionless backfills, while Soubra (2002) extended this to deduce earth pressure coefficients for inclined cohesive-frictional backfills via rotational log spiral failure. Tang et al. (2014) used second-order cone programming in finite-element-based lower-bound limit analysis, revealing its competence in determining coefficients for static and seismic passive earth pressure on inclined rigid retaining walls. This validates lower-bound solutions as reliable passive pressure estimates. Liu et al. (2013) conducted an analytical upper bound limit analysis to offer insights into passive pressure distribution on inclined rough retaining walls with cohesive backfills under uniform surcharges, unearthing correlations between passive earth pressure and soil-wall interface properties. Antao et al. (2011, 2016) harnessed three-dimensional numerical implementations of the upper-bound theorem to establish passive and active earth pressure coefficients. Concurrently, Shiau et al. (2004, 2006) integrated upper-bound and lower-bound theorems, finite elements, and non-linear programming to explore static and seismic pressures on retaining walls and seismic bearing

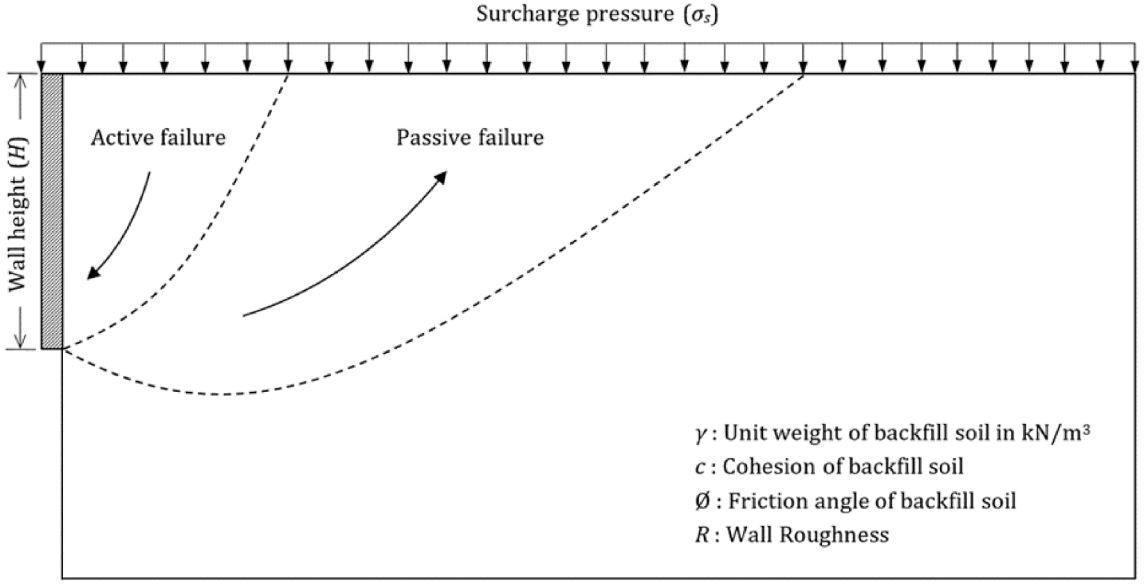

Fig. 1. Problem definition.

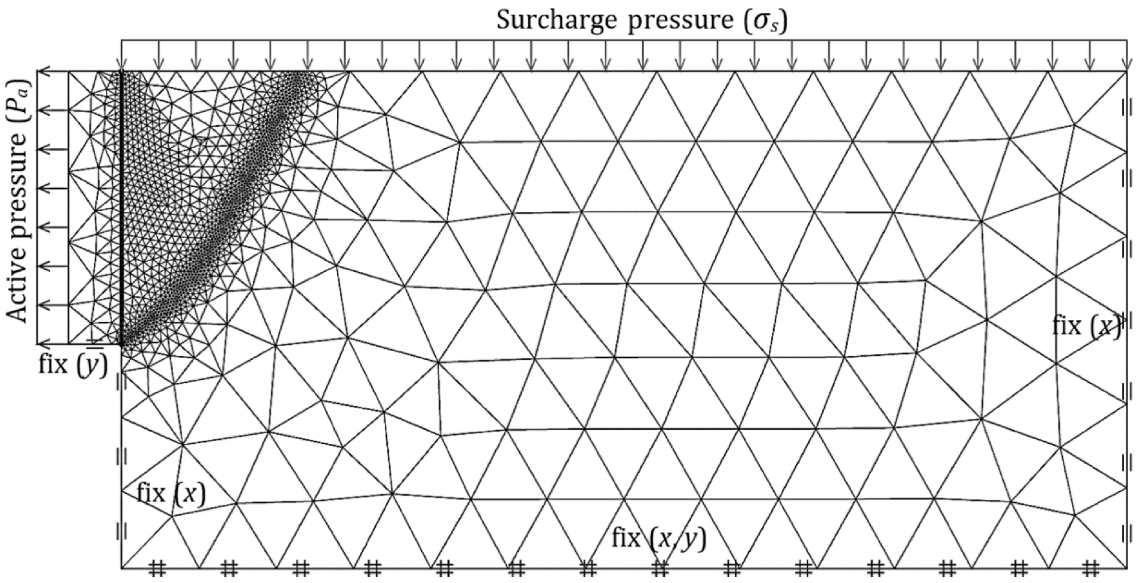

Fig. 2. A typical adaptive mesh and its boundary conditions for the active earth pressure problem (full rough wall $R = 1$, $\phi = 40°$).

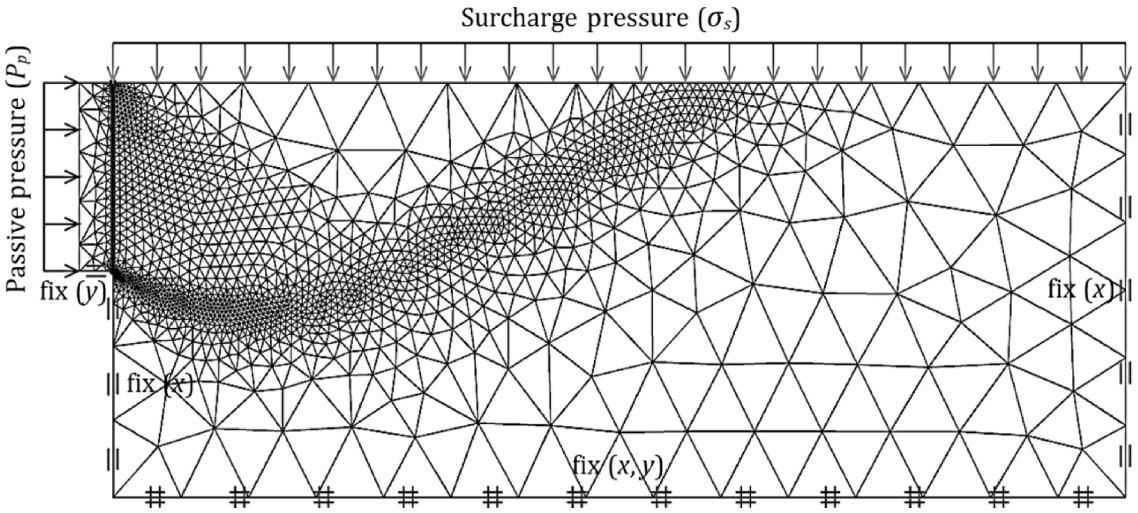

Fig. 3. A typical adaptive mesh and its boundary conditions for the passive earth pressure problem (full rough wall $R = 1$, $\phi = 40°$).

capacity near slopes, effectively delimiting solution ranges. Shiau et al. (2008) conducted a comprehensive study on passive earth pressure, leveraging novel numerical procedures based on upper and lower bounds theorems and non-linear programming. Notably, research using has expanded to include geosynthetic-reinforced retaining structures (Mirmoazen et al. 2021a), structures subjected to anisotropic soil (Mirmoazen et al. 2021b), and nonlinear strength criteria (Li and Yang 2023). However, a research gap remains in solving lateral earth pressure issues in frictional-cohesive soils subjected to surcharges behind rigid retaining walls. This underscores the need for sustained FELA refinements, fostering a comprehensive framework for rigorously determining active and passive earth pressures in these conditions.

Recently, the conservative solutions of lateral active and passive earth pressures exerted on rigid retaining walls have been proposed by Nguyen (2022, 2023a) using a statically admissible stress field for various geometries of wall rear faces and sloping backfills. The solutions are alike to Sokolowski's solution (Sokolovski 1960), and thus they own three main advantages (James and Bransby 1970): (i) a lower-bound type solution, (ii) a high degree of mathematical elegance, (iii) being suitable for the large deformation of soil mass near the wall. These works (Nguyen 2022; Nguyen 2023a) have provided a comprehensive framework to precisely estimate the lateral earth pressures of cohesionless backfill under both active and passive stress states. Furthermore, admissible static stress fields explored in these works could reveal the load transfer mechanism of cohesionless material in the backfill such as soil arching. Therefore, these analytical lower-bound type solutions are adapted to validate the rigorous plastic solution based on FELA.

To date, the accumulation of knowledge surrounding lateral earth pressure has provided a seemingly robust foundation for practical application. Prior research findings indeed serve as dependable solutions for various real-world scenarios, encompassing seismic loading (Bellezza 2014; Choudhury and Nimbalkar 2005; Fathipour et al. 2021a; Fathipour et al. 2021b; Fathipour et al. 2023), intricate backfill compositions, including expansive clayey soil (Pufahl et al. 1983), unsaturated soil behaviour (Vo and Russell 2014, Yang and Chen 2021), and even unsaturated backfills with crack considerations and steady seepage (Zhang et al. 2023). However, within conventional static frameworks, a noticeable research gap persists. A rigorous formulation of active and passive earth pressures that accounts for the intricate interplay between internal frictional angle, soil cohesion, wall roughness, and surcharge loading is conspicuously absent. It is within this context that the significance of the present study is evident. The aim is to pioneer a user-

Table 1
Active F_c vs ϕ for various roughness ($R = 0, 1/3, 1/2, 2/3, 1$).

ϕ	Active F_c									
	$R = 0$		$R = 1/3$		$R = 1/2$		$R = 2/3$		$R = 1$	
	LB	*UB*	*LB*	*UB*	*LB*	*UB*	*LB*	*UB*	*LB*	*UB*
0	2.001	2.001	2.280	2.299	2.385	2.407	2.470	2.493	2.561	2.592
1	1.966	1.982	2.231	2.249	2.330	2.351	2.411	2.433	2.496	2.528
2	1.932	1.948	2.183	2.200	2.277	2.295	2.353	2.373	2.434	2.463
3	1.899	1.913	2.135	2.152	2.225	2.244	2.297	2.316	2.374	2.401
4	1.866	1.880	2.090	2.106	2.174	2.194	2.242	2.262	2.316	2.343
5	1.834	1.848	2.047	2.062	2.125	2.144	2.190	2.209	2.259	2.285
6	1.802	1.816	2.003	2.018	2.079	2.095	2.139	2.157	2.204	2.229
7	1.770	1.785	1.961	1.976	2.032	2.049	2.089	2.106	2.152	2.175
8	1.739	1.753	1.920	1.935	1.988	2.003	2.041	2.058	2.100	2.123
9	1.709	1.722	1.880	1.894	1.945	1.959	1.995	2.010	2.050	2.072
10	1.679	1.691	1.842	1.855	1.902	1.916	1.950	1.965	2.002	2.022
11	1.649	1.661	1.804	1.816	1.861	1.874	1.905	1.920	1.955	1.975
12	1.620	1.631	1.766	1.779	1.820	1.834	1.863	1.877	1.910	1.929
13	1.592	1.603	1.730	1.742	1.781	1.794	1.821	1.836	1.865	1.882
14	1.563	1.574	1.695	1.706	1.743	1.755	1.780	1.794	1.822	1.840
15	1.535	1.546	1.660	1.673	1.706	1.718	1.741	1.755	1.780	1.795
16	1.508	1.519	1.626	1.638	1.669	1.682	1.703	1.714	1.739	1.754
17	1.481	1.489	1.593	1.604	1.633	1.644	1.665	1.676	1.699	1.716
18	1.454	1.465	1.560	1.572	1.599	1.611	1.629	1.639	1.661	1.676
19	1.427	1.438	1.528	1.539	1.565	1.576	1.593	1.603	1.622	1.637
20	1.401	1.412	1.497	1.508	1.532	1.542	1.558	1.570	1.585	1.599
21	1.375	1.387	1.466	1.477	1.499	1.510	1.524	1.533	1.549	1.563
22	1.350	1.359	1.436	1.447	1.467	1.478	1.490	1.501	1.514	1.527
23	1.324	1.335	1.407	1.417	1.436	1.446	1.458	1.468	1.479	1.491
24	1.299	1.310	1.378	1.387	1.405	1.414	1.426	1.435	1.446	1.456
25	1.275	1.285	1.349	1.358	1.375	1.384	1.394	1.404	1.413	1.423
26	1.250	1.258	1.322	1.330	1.346	1.353	1.364	1.373	1.380	1.390
27	1.226	1.234	1.294	1.302	1.317	1.325	1.334	1.342	1.349	1.358
28	1.202	1.210	1.267	1.275	1.289	1.297	1.304	1.311	1.317	1.326
29	1.179	1.186	1.240	1.248	1.261	1.268	1.275	1.283	1.287	1.295
30	1.155	1.163	1.214	1.221	1.234	1.241	1.247	1.254	1.257	1.265
31	1.132	1.141	1.189	1.195	1.207	1.214	1.219	1.226	1.228	1.235
32	1.109	1.116	1.163	1.169	1.180	1.187	1.192	1.198	1.199	1.206
33	1.086	1.095	1.138	1.143	1.154	1.161	1.165	1.171	1.171	1.177
34	1.064	1.070	1.114	1.120	1.129	1.134	1.138	1.144	1.143	1.149
35	1.042	1.047	1.089	1.095	1.104	1.109	1.112	1.118	1.116	1.121
36	1.020	1.027	1.065	1.070	1.079	1.084	1.086	1.092	1.089	1.094
37	0.998	1.003	1.042	1.047	1.054	1.059	1.061	1.066	1.062	1.067
38	0.976	0.981	1.018	1.023	1.030	1.035	1.036	1.042	1.037	1.041
39	0.954	0.960	0.995	1.000	1.006	1.010	1.011	1.016	1.011	1.015
40	0.933	0.938	0.972	0.977	0.982	0.987	0.986	0.991	0.986	0.990

friendly, holistic approach underpinned by three stability factors (F_c, F_s, F_γ), akin to the classical bearing capacity paradigm, for the precise calculation of active and passive thrusts. To accomplish this, the study harnesses the advanced capabilities of the latest Finite Element Limit Analysis (OptumCE, 2020), enhanced by robust adaptive meshing techniques, as the chosen numerical tool to derive rigorous bound solutions. This distinctive methodology emerges as a contribution to the ongoing discourse, with the goal of addressing the nuanced challenges posed by lateral earth pressure computations within static frameworks.

Lastly, it is imperative to emphasize the distinct advantages of our proposed holistic approach, which are underscored through the validation process using several practical examples. These real-world scenarios serve as rigorous test cases to assess the efficacy of our method. In this context, the obtained results for both active and passive thrusts are meticulously subjected to comparison with outcomes derived from established methodologies, including Rankine's method, Coulomb's method, Shields and Tolunay's method, as well as the analytical exact solutions provided by Lancellotta (2007) and Nguyen (2022, 2023a). This extensive comparative analysis is designed with a twofold purpose: first, to affirm the credibility and robustness of our proposed approach.

and second, to juxtapose the accuracy and versatility of our method against well-recognized alternatives. The collective outcomes of these practical examples decisively corroborate the dependability and user-friendliness of our solution in effectively computing lateral earth pressure thrusts. In summary, this study has not only successfully introduced a holistic approach that couples Terzaghi's bearing capacity factors with rigorous FELA techniques for determining static lateral earth pressures but has also demonstrated its superiority through extensive validation and comparison against established methodologies.

2. Problem Scope and Fela Modelling

Although few studies were reported about the estimation of earth pressure using the stability factor approach (F_c, F_s, F_γ), very recently Shiau and Al-Asadi (2020a,b,c) have successfully applied this method to solve a variety of drained and undrained tunnel stability problems in both collapse and blowout scenarios. They adopted an equation, $\left(\sigma_t = -cF_c + \sigma_s F_s + \gamma H F_\gamma\right)$, that is analogous to the three factors $\left(N_c, N_s, N_\gamma\right)$ of bearing capacity equation for strip footings proposed by Terzaghi. Consequently, this superposition approach was chosen in this study to estimate both active and passive earth pressures.

As shown in Fig. 1, the numerical investigation presented in this paper consists of a vertical rigid retaining wall of height H and a horizontal backfill with surcharge σ_s. The backfill soil is taken to be $c-\phi$ Mohr-Coulomb material with unit weight γ. The soil-wall interface roughness is characterized by a reduction factor R, which is a fraction of soil strength parameters. $R = (\tan\delta/\tan\phi) = (c_{int}/c)$, where δ and c_{int} are the interface frictional angle and cohesion, respectively.

Active and passive earth pressure factors due to cohesion (F_c), surcharge loading (F_s), and soil weight (F_γ) are presented for various soil

Table 2
Active F_s vs ϕ for various roughness ($R = 0$, 1/3, 1/2, 2/3, 1).

ϕ	Active F_s									
	$R = 0$		$R = 1/3$		$R = 1/2$		$R = 2/3$		$R = 1$	
	LB	*UB*	*LB*	*UB*	*LB*	*UB*	*LB*	*UB*	*LB*	*UB*
0	0.997	0.997	0.997	0.997	0.997	0.997	0.997	0.997	0.997	0.997
1	0.963	0.963	0.958	0.958	0.957	0.956	0.955	0.955	0.954	0.953
2	0.930	0.929	0.921	0.921	0.918	0.917	0.915	0.915	0.913	0.912
3	0.898	0.897	0.886	0.885	0.881	0.880	0.877	0.876	0.873	0.872
4	0.867	0.866	0.851	0.850	0.846	0.844	0.841	0.840	0.836	0.834
5	0.837	0.836	0.819	0.817	0.812	0.810	0.806	0.805	0.800	0.798
6	0.808	0.807	0.787	0.786	0.779	0.778	0.773	0.771	0.766	0.764
7	0.780	0.779	0.757	0.755	0.748	0.746	0.741	0.739	0.734	0.731
8	0.753	0.751	0.728	0.726	0.719	0.717	0.711	0.709	0.703	0.700
9	0.727	0.725	0.700	0.698	0.690	0.688	0.682	0.680	0.673	0.670
10	0.702	0.699	0.673	0.671	0.663	0.661	0.654	0.652	0.645	0.642
11	0.677	0.675	0.648	0.645	0.637	0.634	0.628	0.625	0.618	0.611
12	0.653	0.651	0.623	0.620	0.612	0.609	0.603	0.599	0.592	0.589
13	0.630	0.628	0.599	0.597	0.588	0.585	0.578	0.575	0.568	0.563
14	0.608	0.605	0.576	0.574	0.564	0.561	0.555	0.552	0.544	0.540
15	0.587	0.584	0.554	0.552	0.542	0.539	0.532	0.529	0.521	0.517
16	0.566	0.563	0.533	0.530	0.521	0.517	0.511	0.508	0.500	0.495
17	0.545	0.542	0.513	0.510	0.500	0.497	0.490	0.487	0.479	0.474
18	0.526	0.523	0.493	0.490	0.481	0.477	0.471	0.467	0.459	0.454
19	0.507	0.504	0.474	0.471	0.462	0.458	0.452	0.448	0.440	0.435
20	0.488	0.484	0.456	0.453	0.443	0.440	0.433	0.430	0.421	0.417
21	0.470	0.466	0.438	0.435	0.426	0.422	0.416	0.412	0.404	0.399
22	0.453	0.449	0.421	0.418	0.409	0.406	0.399	0.395	0.387	0.382
23	0.436	0.432	0.404	0.401	0.392	0.389	0.382	0.379	0.371	0.366
24	0.420	0.417	0.389	0.385	0.377	0.373	0.367	0.363	0.355	0.350
25	0.404	0.401	0.373	0.370	0.361	0.358	0.352	0.348	0.340	0.335
26	0.389	0.385	0.358	0.355	0.347	0.344	0.337	0.334	0.325	0.321
27	0.374	0.371	0.344	0.341	0.333	0.330	0.323	0.321	0.312	0.307
28	0.359	0.356	0.330	0.327	0.319	0.316	0.310	0.307	0.298	0.294
29	0.345	0.341	0.317	0.314	0.306	0.303	0.297	0.294	0.286	0.281
30	0.332	0.328	0.304	0.301	0.293	0.291	0.284	0.281	0.273	0.269
31	0.318	0.315	0.292	0.289	0.281	0.278	0.272	0.269	0.261	0.257
32	0.306	0.302	0.280	0.276	0.269	0.267	0.261	0.258	0.250	0.246
33	0.293	0.290	0.268	0.265	0.258	0.255	0.250	0.246	0.239	0.234
34	0.281	0.278	0.257	0.254	0.247	0.244	0.239	0.236	0.228	0.224
35	0.269	0.266	0.246	0.243	0.236	0.233	0.228	0.225	0.218	0.215
36	0.258	0.255	0.235	0.232	0.226	0.223	0.218	0.215	0.210	0.203
37	0.247	0.244	0.225	0.222	0.216	0.213	0.209	0.205	0.198	0.194
38	0.236	0.233	0.215	0.212	0.206	0.204	0.199	0.196	0.189	0.185
39	0.226	0.223	0.206	0.203	0.197	0.194	0.190	0.187	0.180	0.177
40	0.216	0.213	0.196	0.193	0.189	0.185	0.182	0.179	0.172	0.168

internal friction angles (ϕ) and wall roughness (R). Accordingly, the average pressures acting on the wall (obtained by FELA) for active earth pressure (p_a) and passive earth pressure (p_p) are shown in equations (1) and (2), respectively.

$$p_a = -cF_c + \sigma_s F_s + \gamma H F_\gamma \tag{1}$$

$$p_p = cF_c + \sigma_s F_s + \gamma H F_\gamma \tag{2}$$

where c is the effective cohesion, σ_s is the intensity of the possible surcharge loading on the ground surface, γ is the soil unit weight, and H is the height of the retaining wall.

With the wall height H, the total active thrust (P_A) and passive thrust (P_P) acting on the retaining wall are presented in equations (3) and (4) respectively.

$$P_A = -cF_cH + \sigma_s F_s H + \gamma H^2 F_\gamma \tag{3}$$

$$P_P = cF_cH + \sigma_s F_s H + \gamma H^2 F_\gamma \tag{4}$$

Finite Element Limit Analysis (FELA) is a numerical computational process of limit analysis that uses classical plasticity theorems with the concept of both finite elements and mathematical programming (Sloan 2013). The rigorous upper bound (*UB*) and lower bound (*LB*) limit theorems are particularly effective when both types of solution are calculated simultaneously so that the actual ultimate load can be bracketed from above and below. The difference between these two limits then provides an accurate measurement of the discrete error in the solution and can be used to improve the meshes until an adequate and precise estimate of the failure load is found (Sloan 2013). The code, OptumG2, has recently been successfully applied to several geotechnical stability problems (see for examples, Ukritchon and Keawsawasvong 2018.

Keawsawasvong and Ukritchon 2019. Krabbenhoft 2018, 2019.

Shiau et al. 2022), and it is adopted in the paper to compute the active and passive earth pressure factors (F_c, F_s, F_γ).

Figs. 2 and 3 show two typical FELA meshes and their boundary conditions used in the active and passive failure analyses respectively. The boundary conditions of the meshes were defined such that the bottom boundary of the model is fixed in both vertical and horizontal directions, whereas the left and right boundaries of the problem are allowed to move only in the vertical direction. The face of the vertical rigid retaining wall is subject to uniform active translation (wall moves away from the soil) to induce an active failure or uniform passive translation (wall moves towards the soil) to induce a passive failure. The size of the problem domains is selected to be large enough so that the plastic yielding zone be contained within the domain.

An automatically adaptive mesh refinement based on shear dissipation was employed to calculate the tight *UB* and *LB* solutions. Three adaptive refinement steps are selected by increasing the number of elements from 3,000 elements in the first step to approximately 5,000 elements in the final step. The examples of final adaptive meshes after

Table 3
Active F_γ vs ϕ for various roughness ($R = 0, 1/3, 1/2, 2/3, 1$). Note - $K_\gamma = 2F_\gamma$.

ϕ	Active F_γ									
	$R = 0$		$R = 1/3$		$R = 1/2$		$R = 2/3$		$R = 1$	
	LB	*UB*	*LB*	*UB*	*LB*	*UB*	*LB*	*UB*	*LB*	*UB*
0	0.500	0.500	0.500	0.500	0.500	0.500	0.500	0.500	0.500	0.500
1	0.483	0.483	0.480	0.480	0.479	0.479	0.479	0.478	0.477	0.477
2	0.466	0.466	0.462	0.461	0.460	0.459	0.458	0.458	0.456	0.455
3	0.450	0.450	0.444	0.443	0.441	0.441	0.439	0.438	0.436	0.435
4	0.435	0.434	0.427	0.426	0.425	0.423	0.420	0.420	0.416	0.415
5	0.420	0.419	0.410	0.409	0.406	0.405	0.403	0.402	0.398	0.397
6	0.405	0.404	0.394	0.393	0.390	0.389	0.386	0.385	0.381	0.379
7	0.391	0.390	0.379	0.378	0.374	0.373	0.370	0.369	0.364	0.363
8	0.378	0.376	0.365	0.363	0.359	0.358	0.355	0.354	0.348	0.347
9	0.363	0.365	0.349	0.351	0.344	0.345	0.339	0.340	0.332	0.333
10	0.352	0.350	0.337	0.336	0.331	0.330	0.326	0.325	0.319	0.317
11	0.340	0.338	0.324	0.323	0.318	0.317	0.313	0.311	0.305	0.304
12	0.328	0.326	0.312	0.310	0.306	0.304	0.300	0.298	0.292	0.290
13	0.316	0.314	0.300	0.298	0.294	0.292	0.288	0.286	0.280	0.278
14	0.305	0.304	0.289	0.287	0.282	0.280	0.276	0.275	0.268	0.266
15	0.294	0.292	0.277	0.276	0.271	0.269	0.265	0.263	0.257	0.254
16	0.284	0.282	0.267	0.265	0.260	0.258	0.254	0.253	0.246	0.244
17	0.274	0.272	0.257	0.255	0.250	0.248	0.244	0.242	0.234	0.233
18	0.264	0.262	0.247	0.245	0.240	0.238	0.234	0.232	0.225	0.223
19	0.254	0.252	0.237	0.235	0.230	0.228	0.225	0.223	0.216	0.214
20	0.245	0.242	0.228	0.226	0.221	0.219	0.215	0.213	0.207	0.204
21	0.236	0.234	0.219	0.217	0.213	0.211	0.207	0.205	0.198	0.196
22	0.227	0.225	0.211	0.209	0.204	0.202	0.198	0.196	0.190	0.187
23	0.219	0.217	0.203	0.200	0.196	0.194	0.190	0.188	0.182	0.179
24	0.211	0.209	0.195	0.192	0.188	0.186	0.182	0.180	0.174	0.172
25	0.203	0.200	0.187	0.185	0.181	0.179	0.175	0.173	0.166	0.164
26	0.195	0.193	0.180	0.178	0.173	0.171	0.168	0.166	0.159	0.157
27	0.188	0.185	0.172	0.170	0.166	0.164	0.161	0.159	0.152	0.150
28	0.181	0.177	0.166	0.163	0.159	0.157	0.154	0.152	0.146	0.144
29	0.174	0.171	0.159	0.157	0.153	0.151	0.148	0.146	0.139	0.137
30	0.167	0.163	0.152	0.150	0.147	0.145	0.142	0.139	0.133	0.131
31	0.160	0.157	0.146	0.144	0.141	0.138	0.136	0.134	0.128	0.126
32	0.154	0.151	0.140	0.138	0.135	0.133	0.130	0.128	0.122	0.120
33	0.147	0.145	0.134	0.132	0.129	0.127	0.124	0.122	0.116	0.114
34	0.141	0.139	0.129	0.127	0.123	0.122	0.119	0.117	0.111	0.109
35	0.136	0.133	0.123	0.121	0.118	0.116	0.114	0.112	0.106	0.104
36	0.130	0.126	0.118	0.116	0.113	0.111	0.109	0.107	0.101	0.100
37	0.124	0.122	0.113	0.111	0.108	0.106	0.104	0.102	0.097	0.095
38	0.119	0.115	0.108	0.106	0.103	0.101	0.099	0.097	0.092	0.090
39	0.114	0.109	0.103	0.101	0.099	0.097	0.095	0.093	0.088	0.086
40	0.109	0.104	0.099	0.096	0.094	0.092	0.090	0.089	0.084	0.082

three adaptive refinement steps are shown in Figs. 2 and 3 for active and passive studies, respectively.

The active or passive earth pressures are optimised in both upper and lower bound simulations to compute the bound solution of the three stability factors (F_c, F_s, F_γ). The principles of these calculations using Equations (1) and (2) are as follows.

1. To determine active and passive factors F_c, both (γ=0 and$\sigma_s = 0$) are used in the analysis to obtain p_a and p_p. The active and passive F_c factors are then calculated using $p_a = -cF_c$ and $p_p = cF_c$ respectively.
2. To determine active and passive factors F_s, ($c = 0$ and$\gamma = 0$) are used in the analysis. The active and passive F_s factors are then calculated using the equations $p_a = \sigma_s F_s$ and $p_p = \sigma_s F_s$ respectively, once p_a and p_p are computed in the FELA.
3. To determine active and passive factors F_γ, both ($c = 0$ and$\sigma_s = 0$) are used in the analysis to compute p_a and p_p. The active and passive F_γ factors can then be calculated using the equations $p_a = \gamma H F_\gamma$ and $p_p = \gamma H F_\gamma$ respectively.

Using the principle of superposition, the minimum support pressure (p_a or p_p) at collapse can be determined for a wide range of soil parameters such as angles of internal friction (ϕ=0° – 40°) and wall roughness (R=0, 1/3, 1/2, 2/3, 1).

3. Active Earth Pressure Factors (F_C, F_S, and F_γ)

Complete numerical results of active (F_c, F_s, and F_γ) are tabulated in Tables 1-3, and graphically presented in Figs. 4-6. Below are the discussions for their respective effects.

3.1. the cohesion factor, F_c

Assuming no surcharge pressure ($\sigma_S = 0$) and an idealised weightless soil ($\gamma = 0$), a total of 410 FELA was performed to compute the active F_c using equation (1). Numerical results of F_c are shown in Fig. 4 to demonstrate the effect of ϕ versus F_c for a range of R. It is not surprising to see that F_c decreases as the angle of internal friction (ϕ) increases. The effect of soil cohesion diminishes as the soil friction angle increases. The larger the roughness value (R) is, the greater the F_c. The difference between rough and smooth F_c becomes small as the soil friction angle increases. Noting the negative sign in equation (1), the results indicate that less active force on the force when the wall is rough.

3.2. the surcharge factor, F_s

To calculate active surcharge factors F_s using Equation (1), it is necessary to use ($c = 0$) and ($\gamma = 0$) in all 410 FELA analyses. Fig. 5 shows that the maximum value of active F_s is equal to one at $\phi = 0°$, and it dramatically decreases as the internal friction angle of soil (ϕ) increases.

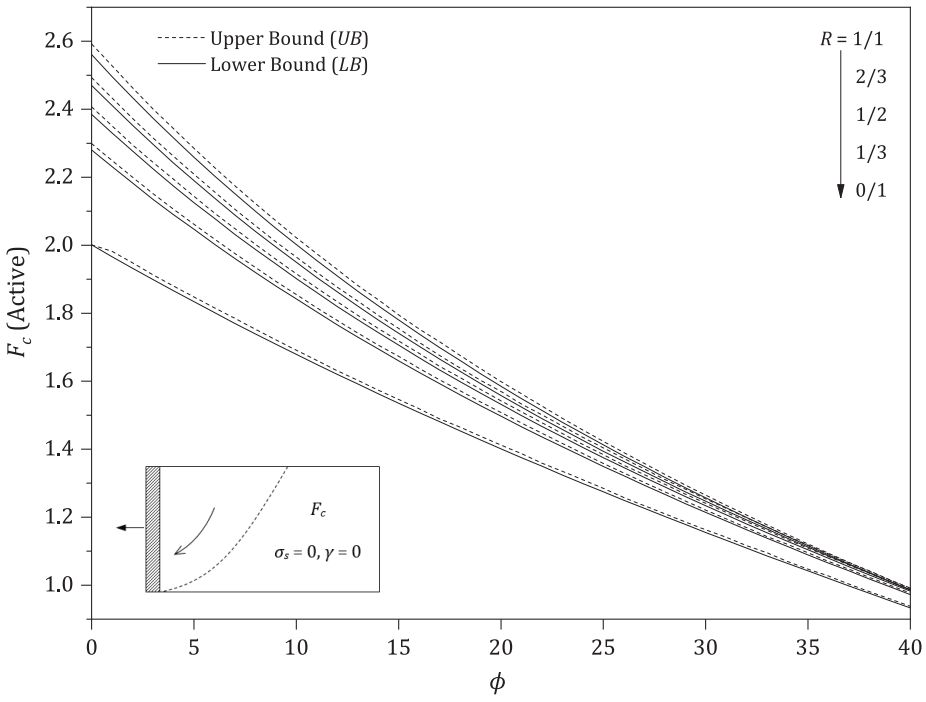

Fig. 4. Active F_c vs ϕ for various wall roughness.

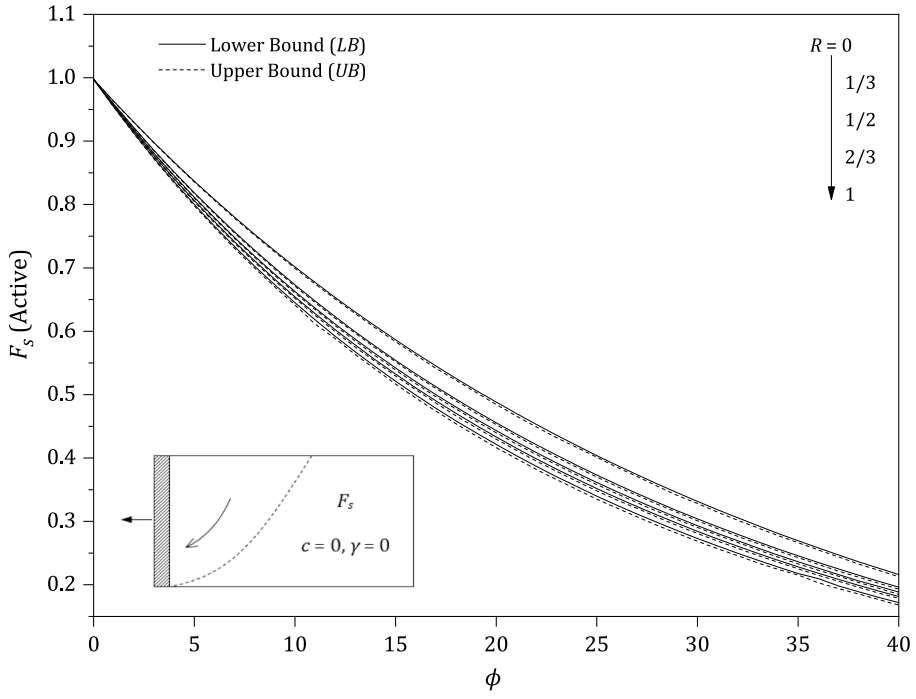

Fig. 5. Active F_s vs ϕ for various wall roughness.

It may be concluded that the surcharge pressure σ_s has very little contribution to the active earth pressure when the value of ϕ is large. Besides the effect of roughness is small and can be ignored. As expected, the assumption of a smooth wall in design practice would produce a conservative outcome.

3.3. the unit weight factor, F_γ

The effect ϕ on the unit weight factor F_γ is presented in Fig. 6 for various wall roughness (R). The results were obtained by using ($c = 0$) and ($\sigma_s = 0$) in all 410 analyses. Fig. 6 shows that the maximum value of active F_γ is equal to 0.5 at $\phi = 0^{\circ}$, and it decreases dramatically as the soil friction angle ϕ increases. The effect of unit weight (or the overburden pressure) decreases as the soil friction angle increases. This is possibly due to the development of soil arching as the value of ϕ increases. In addition, F_γ in the smooth wall ($R = 0$) is greater than those associated with the perfectly rough wall ($R = 1$), although the differences can be ignored. Again, the use of a smooth wall in design would yield larger

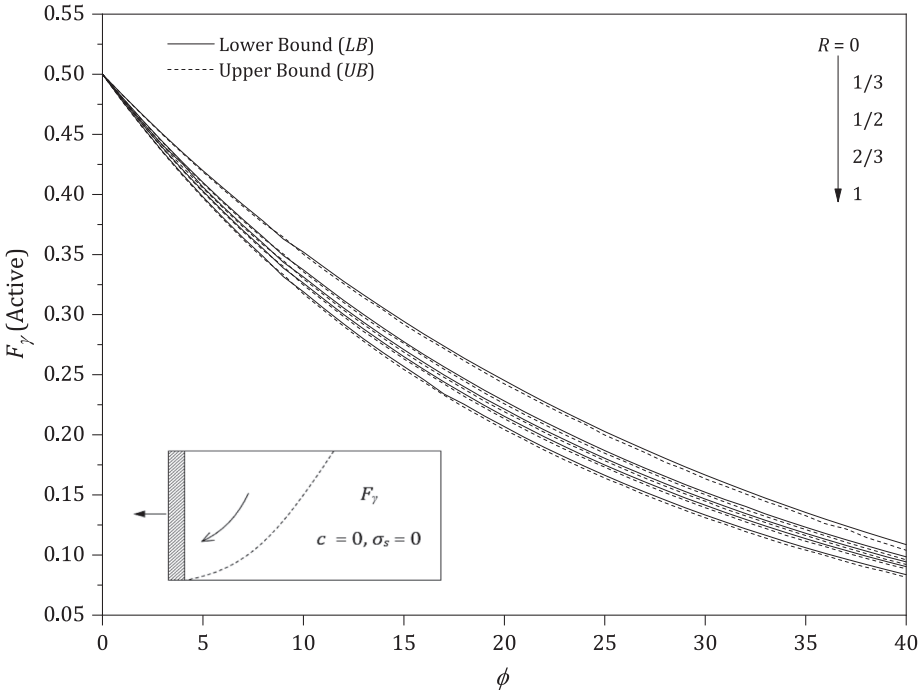

Fig. 6. Active F_γ vs ϕ for various wall roughness.

active earth pressure and therefore it is a conservative design assumption.

4. Passive Earth Pressure Factors (F_C, F_S, and F_γ)

A comprehensive result of passive factors (F_c, F_s, F_γ) are tabulated in Tables 4-6 and presented graphically in Figs. 7-9. The effects of the respective passive earth pressure factors are discussed below.

4.1. the cohesion factor, F_c

Similar to the active cases, passive factors F_c were produced based on the assumption of ($\sigma_S = 0$) and ($\gamma = 0$). Equation (2) reduces to $F_c = p_p/c$, and it can be used to calculate the factors. Fig. 7 shows that the larger the roughness value (R) is, the greater the F_c, and therefore the greater the passive earth pressure. It is important to note the large difference in F_c between perfectly rough and smooth walls when the friction angle of backfill soil (ϕ) is 40°. It is conservative to adopt a smooth wall in the design of a passive wall.

4.2. the surcharge factor, F_s

To obtain passive surcharge factors F_s, it is necessary to use ($c = 0$) and ($\gamma = 0$) in the analysis. A total of 410 runs of FELA were performed to compute passive F_s using $F_s = p_p/\sigma_s$. Fig. 8 shows that the larger the wall roughness R value, the greater the passive surcharge factor F_s. Note that the minimum value of passive F_s is unity at $\phi = 0°$, and it increases dramatically as the internal friction angle (ϕ) of the soil increases. It can therefore be concluded that the passive surcharge pressure σ_s contribute significantly to the total passive resistance when the value of ϕ is large. This is opposite to the active wall, where an increase of ϕ results in a significant decrease in the active F_s as well as the active pressure on the wall.

4.3. the unit weight factor, F_γ

The effects of ϕ and R on the passive factor F_γ are presented in Fig. 9. Similarly, the results can be obtained by using ($c = 0$) and ($\sigma_s = 0$) in the analyses. The results have shown that the minimum value of passive F_γ is equal to 0.5 at $\phi = 0°$, and it increases dramatically as the soil friction angle ϕ increases. The larger the ϕ and the R, the greater the passive F_γ is, and therefore the greater the passive earth pressure is. The effect of R is large, and it cannot be ignored, especially for large values of ϕ. As before, it is conservative to adopt a smooth wall in the design of a passive wall.

5. Validation with Analytical Lower-Bound Type Solutions

5.1. Analytical solution based on rigid-plasticity behaviour

The problem formulation is presented in Fig. 10. Denoting that the backfill is made of a cohesionless soil without surcharge, everywhere in the backfill is on the verge of incipient failure complies with the Mohr-Coulomb yield criterion, and thus the following expression (ref. Eq. (5)) is satisfied everywhere in the backfill,

$$(\sigma_r - \sigma_\theta)^2 + 4\tau_{r\theta}^2 = (\sigma_r + \sigma_\theta)^2 \sin^2\phi \tag{5}$$

The relative angle of the major principal stress (ψ) and in-plane mean stress (p) is adopted to conveniently express stress components in the polar coordinate system. Since everywhere in the backfill is on the verge of incipient failure obeying the yield criterion (ref. Eq. (5)), the expression of the stress components is given as,

$$\begin{cases} \sigma_{rr} = p(1 + \sin\phi\cos 2\psi) \\ \sigma_{\theta\theta} = p(1 - \sin\phi\cos 2\psi) \\ \tau_{r\theta} = p\sin\phi\sin 2\psi \end{cases} \tag{6}$$

where p is average normal stress, $p = (\sigma_{rr} + \sigma_{\theta\theta})/2$.

Denoted that the relative angle of the major principal stress (ψ) and in-plane mean stress (p) are two functions concerning the variable of angular coordinate (θ). Owing to the self-similarity assumption (Sokolovskii (1965)), the radial stress field is postulated as follows,

$$p = \gamma r \chi(\theta) \tag{7}$$

$$\psi = \psi(\theta) \tag{8}$$

Table 4
Passive F_c vs ϕ for various roughness (R = 0, 1/3, 1/2, 2/3, 1).

ϕ	Passive F_c									
	$R = 0$		$R = 1/3$		$R = 1/2$		$R = 2/3$		$R = 1$	
	LB	*UB*	*LB*	*UB*	*LB*	*UB*	*LB*	*UB*	*LB*	*UB*
0	2.001	2.018	2.281	2.300	2.385	2.408	2.470	2.493	2.561	2.592
1	2.036	2.054	2.330	2.350	2.442	2.465	2.532	2.556	2.628	2.662
2	2.072	2.089	2.383	2.403	2.503	2.525	2.596	2.622	2.698	2.734
3	2.109	2.127	2.437	2.458	2.564	2.578	2.663	2.690	2.770	2.809
4	2.146	2.164	2.493	2.515	2.627	2.651	2.731	2.760	2.844	2.885
5	2.184	2.202	2.550	2.573	2.693	2.718	2.802	2.834	2.922	2.965
6	2.222	2.241	2.610	2.635	2.760	2.787	2.878	2.908	3.004	3.048
7	2.262	2.281	2.670	2.696	2.831	2.858	2.955	2.990	3.088	3.139
8	2.302	2.321	2.735	2.761	2.903	2.936	3.037	3.072	3.177	3.229
9	2.343	2.363	2.800	2.828	2.979	3.011	3.121	3.157	3.268	3.325
10	2.385	2.406	2.865	2.897	3.058	3.089	3.209	3.246	3.364	3.424
11	2.427	2.451	2.936	2.970	3.139	3.175	3.299	3.340	3.464	3.527
12	2.471	2.494	3.010	3.046	3.223	3.262	3.395	3.438	3.570	3.635
13	2.516	2.540	3.084	3.118	3.314	3.352	3.493	3.537	3.680	3.756
14	2.561	2.586	3.162	3.199	3.406	3.448	3.595	3.645	3.793	3.874
15	2.608	2.634	3.249	3.285	3.493	3.545	3.707	3.757	3.915	4.002
16	2.655	2.680	3.335	3.374	3.599	3.651	3.820	3.877	4.038	4.132
17	2.704	2.729	3.423	3.457	3.705	3.762	3.941	4.003	4.179	4.279
18	2.754	2.781	3.516	3.559	3.817	3.873	4.064	4.126	4.320	4.415
19	2.805	2.832	3.606	3.657	3.931	3.982	4.192	4.262	4.471	4.576
20	2.858	2.886	3.706	3.752	4.057	4.116	4.325	4.411	4.619	4.746
21	2.911	2.943	3.811	3.868	4.183	4.242	4.472	4.554	4.791	4.925
22	2.967	2.996	3.922	3.974	4.318	4.380	4.632	4.726	4.966	5.103
23	3.023	3.058	4.036	4.096	4.452	4.531	4.796	4.895	5.163	5.305
24	3.081	3.114	4.154	4.210	4.601	4.682	4.967	5.063	5.355	5.513
25	3.141	3.173	4.282	4.339	4.762	4.851	5.149	5.269	5.567	5.741
26	3.202	3.237	4.417	4.490	4.925	5.019	5.354	5.460	5.794	5.965
27	3.265	3.301	4.552	4.618	5.099	5.211	5.548	5.674	6.016	6.227
28	3.330	3.369	4.698	4.767	5.277	5.385	5.769	5.908	6.271	6.506
29	3.397	3.437	4.847	4.927	5.490	5.600	5.993	6.149	6.560	6.801
30	3.466	3.514	5.013	5.102	5.700	5.824	6.256	6.410	6.856	7.103
31	3.537	3.582	5.177	5.266	5.904	6.056	6.523	6.697	7.165	7.465
32	3.610	3.660	5.356	5.459	6.118	6.302	6.808	6.989	7.502	7.817
33	3.685	3.737	5.550	5.652	6.398	6.554	7.119	7.328	7.879	8.218
34	3.763	3.812	5.744	5.866	6.663	6.837	7.454	7.681	8.286	8.648
35	3.844	3.897	5.968	6.086	6.965	7.158	7.779	8.053	8.706	9.131
36	3.927	3.972	6.201	6.325	7.262	7.472	8.187	8.480	9.202	9.648
37	4.013	4.061	6.437	6.602	7.610	7.822	8.598	8.961	9.685	10.230
38	4.103	4.165	6.691	6.856	7.950	8.213	9.017	9.402	10.270	10.820
39	4.195	4.257	6.978	7.145	8.330	8.627	9.536	9.911	10.890	11.570
40	4.291	4.345	7.272	7.455	8.756	9.063	10.080	10.530	11.550	12.320

By all means, all stress components must satisfy the equilibrium equations everywhere,

$$\frac{\partial \sigma_{rr}}{\partial r}+\frac{1}{r}\frac{\partial \tau_{r\theta}}{\partial \theta}+\frac{\sigma_{rr}-\sigma_{\theta\theta}}{r}=\gamma\cos\theta \tag{9}$$

$$\frac{\partial \tau_{r\theta}}{\partial r}+\frac{1}{r}\frac{\partial \sigma_{\theta\theta}}{\partial \theta}+2\frac{\tau_{r\theta}}{r}=-\gamma\sin\theta \tag{10}$$

Substituting the stress components given in Eq. (6) together with the self-similarity assumption (expressed in Eqs. (7)-(8)) into the equilibrium equations (Eqs. (9)-(10)), a new form of the equilibrium equations is formulated consisting of the two variables (χ) and (ψ),

$$\sin\phi\sin2\psi\frac{d\chi}{d\theta}+2\chi\sin\phi\cos2\psi\left(\frac{d\psi}{d\theta}+1\right)+\chi(1+\sin\phi\cos2\psi)=\cos\theta \tag{11}$$

$$(1-\sin\phi\cos2\psi)\frac{d\chi}{d\theta}+2\chi\sin\phi\sin2\psi\left(\frac{d\psi}{d\theta}+1\right)+\chi\sin\phi\sin2\psi=-\sin\theta \tag{12}$$

Rearranging Eqs. (11) - (12), the governing equations, which are a pair of Ordinary Differential Equations (ODEs), are given as follows,

$$\frac{d\chi}{d\theta}=\frac{\chi(\theta)\sin(2\psi)-\sin(2\psi+\theta)}{\cos2\psi-\sin\phi} \tag{13}$$

$$\frac{d\Psi}{d\theta}=\frac{d\psi}{d\theta}+1=\frac{\sin\phi\cos(2\psi+\theta)+\chi(\theta)\cos^2\phi-\cos\theta}{2\chi(\theta)\sin\phi(\sin\phi-\cos2\psi)} \tag{14}$$

Considering the wall roughness, the following conditions are assumed to exist at the wall's rear face ($\theta = 0$) for positive wall-soil friction under the a priori stress conditions of active and passive states given in Eq. (15) and (16), respectively (Nguyen 2022, 2023a).

$$\tau_{r\theta}=-\sigma_{rr}\tan\delta \tag{15}$$

$$\tau_{r\theta}=\sigma_{\theta}\tan\delta \tag{16}$$

The stress components expressed in Eq. (6) are substituted into Eq. (15) and (16), thus the initial boundary condition on the relative angle of the major principal stress (ψ) is derived at the wall rear face ($\theta = 0$) for active and passive earth pressure as follows,

$$\psi_w=\frac{1}{2}\left[\delta+\arcsin\left(\frac{-\sin\delta}{\sin\phi}\right)\right] \tag{17}$$

$$\psi_w=\frac{1}{2}\left[\pi-\delta-\arcsin\left(\frac{\sin\delta}{\sin\phi}\right)\right] \tag{18}$$

The above problem formulation enables the statically admissible stress field to be developed in the backfill. This static stress field is found by employing robust numerical frameworks which are well documented in Nguyen (2022, 2023a, 2023b). Overall, it should be noted that the Rankine region does not appear in the entire backfill since the backfill is separated into two regions i.e., Rankine region and non-Rankine region, by a line of stress singularity (Nguyen and Pipatpongsa 2020). Thus,

Table 5
Passive F_s vs ϕ for various roughness ($R = 0$, 1/3, 1/2, 2/3, 1).

ϕ	Passive F_s									
	$R = 0$		$R = 1/3$		$R = 1/2$		$R = 2/3$		$R = 1$	
	LB	*UB*	*LB*	*UB*	*LB*	*UB*	*LB*	*UB*	*LB*	*UB*
0	1.003	1.003	1.003	1.003	1.003	1.003	1.003	1.003	1.003	1.003
1	1.039	1.039	1.043	1.044	1.045	1.046	1.047	1.047	1.049	1.049
2	1.075	1.076	1.086	1.087	1.090	1.091	1.093	1.094	1.097	1.098
3	1.114	1.115	1.131	1.132	1.137	1.138	1.142	1.144	1.148	1.150
4	1.153	1.154	1.177	1.179	1.187	1.188	1.194	1.196	1.202	1.204
5	1.194	1.196	1.226	1.228	1.238	1.241	1.248	1.251	1.259	1.262
6	1.237	1.239	1.277	1.280	1.293	1.296	1.305	1.309	1.319	1.323
7	1.281	1.283	1.331	1.334	1.351	1.354	1.366	1.370	1.382	1.388
8	1.327	1.330	1.387	1.391	1.411	1.415	1.429	1.435	1.450	1.457
9	1.374	1.378	1.447	1.451	1.475	1.480	1.497	1.503	1.521	1.529
10	1.424	1.427	1.509	1.514	1.542	1.548	1.569	1.575	1.596	1.607
11	1.475	1.479	1.574	1.580	1.613	1.620	1.644	1.652	1.677	1.689
12	1.529	1.533	1.642	1.650	1.689	1.696	1.725	1.733	1.762	1.777
13	1.584	1.590	1.715	1.722	1.768	1.776	1.809	1.820	1.853	1.870
14	1.642	1.648	1.791	1.800	1.850	1.862	1.899	1.911	1.950	1.970
15	1.702	1.709	1.871	1.882	1.939	1.953	1.996	2.009	2.054	2.075
16	1.765	1.772	1.958	1.968	2.034	2.050	2.099	2.113	2.165	2.190
17	1.830	1.838	2.046	2.060	2.134	2.152	2.208	2.226	2.282	2.311
18	1.899	1.908	2.142	2.157	2.241	2.258	2.320	2.343	2.407	2.439
19	1.970	1.980	2.242	2.257	2.355	2.372	2.447	2.468	2.544	2.580
20	2.044	2.054	2.349	2.367	2.476	2.497	2.576	2.603	2.690	2.731
21	2.121	2.133	2.463	2.482	2.605	2.627	2.719	2.748	2.844	2.895
22	2.202	2.214	2.583	2.605	2.743	2.767	2.871	2.905	3.011	3.064
23	2.287	2.301	2.710	2.733	2.887	2.917	3.035	3.076	3.193	3.253
24	2.376	2.390	2.845	2.876	3.045	3.084	3.210	3.252	3.389	3.458
25	2.469	2.486	2.992	3.020	3.215	3.255	3.398	3.449	3.603	3.681
26	2.566	2.585	3.147	3.176	3.396	3.437	3.603	3.658	3.831	3.922
27	2.668	2.688	3.312	3.348	3.589	3.637	3.824	3.889	4.080	4.175
28	2.775	2.796	3.487	3.534	3.803	3.857	4.064	4.133	4.344	4.460
29	2.887	2.912	3.676	3.717	4.026	4.097	4.321	4.401	4.642	4.775
30	3.005	3.028	3.880	3.931	4.271	4.350	4.613	4.693	4.958	5.106
31	3.129	3.156	4.099	4.161	4.532	4.621	4.902	5.018	5.315	5.478
32	3.260	3.283	4.326	4.400	4.819	4.919	5.238	5.366	5.702	5.886
33	3.398	3.430	4.587	4.647	5.133	5.231	5.614	5.745	6.137	6.356
34	3.543	3.572	4.864	4.930	5.479	5.583	6.005	6.164	6.604	6.839
35	3.696	3.733	5.149	5.232	5.843	5.977	6.436	6.625	7.109	7.420
36	3.858	3.890	5.470	5.561	6.254	6.391	6.936	7.123	7.674	8.002
37	4.029	4.065	5.811	5.914	6.689	6.849	7.448	7.688	8.334	8.718
38	4.210	4.248	6.190	6.320	7.158	7.372	8.043	8.309	9.040	9.462
39	4.402	4.440	6.598	6.748	7.711	7.916	8.679	8.998	9.820	10.320
40	4.605	4.652	7.045	7.200	8.292	8.531	9.426	9.764	10.730	11.300

correctly determining the line of stress singularity is critical to successfully figuring out the admissible stress field using the two-step numerical framework developed by Nguyen (2022, 2023a).

5.2. Validation of F_γ under both active and passive earth pressures

At first, the results of the unit weight factor (F_γ) obtained by this study are compared with those of the conservative solutions for both active and passive earth pressures as shown in Fig. 11 and Fig. 12, respectively. The perfect agreement between the two solutions is observed in active earth pressure (ref. Fig. 11). Despite a slight discrepancy observed in passive earth pressure (ref. Fig. 12), the unit weight factor (F_γ) provided by both solutions under passive earth pressure is still comparable to each other. This comparison rigorously justifies the accuracy and reliability of the proposed solution in proving the unit weight factor (F_γ).

The load transfer mechanism in cohesionless backfill under the activation of active and passive earth pressures has been investigated by several researchers. The works dedicated by James and Bransby (1970) and Nguyen (2022) on exploring the direction of the major principal stress in cohesionless backfill under passive earth pressure are noticeable. Thus, the directions of principal stresses achieved by the proposed FELA are compared with those of past studies (see Fig. 13 and Fig. 14).

Fig. 13 demonstrates the directions of principal stresses in the case of a smooth wall. Both FELA and the analytical lower-bound type solution yield the same feature of load transfer mechanism in the backfill in the absence of the wall's roughness. The direction of the major principal stress is exactly horizontal in the backfill (ref. Fig. 13). Conversely, the presence of the wall's roughness substantially rotated the direction of the major principal stress from a horizontal direction to downward a diagonal direction (ref. Fig. 14). These traits of the load transfer mechanism are similarly observed in the three solutions i.e., FELA (see Fig. 14(a)), analytical lower-bound type solution (see Fig. 14(b)), and experimental observation (see Fig. 14(c)). This perfect agreement on exploring the traits of load transfer mechanism in cohesionless backfill under passive stress state further convinces the accuracy of the proposed approach. Moreover, by showing the rotating direction of the major principal stress induced by the wall roughness, the effect of wall roughness on the magnitude of active and passive thrust exerted on a retaining wall has been elucidated thereof. By comparing the performance of FELA using OPTUM G2 with the analytical and experimental approaches, the superiority of FELA in accurately determining the lateral earth pressure values for a wide range of soil profiles has been established. Additionally, FELA has the unique advantage of elucidating the load transfer mechanism by analyzing the characteristics of major principal stress. This comprehensive approach provides valuable insights into the behavior of soil structures and enhances our understanding of their stability and performance.

Table 6
Passive F_γ vs ϕ for various roughness ($R = 0$, 1/3, 1/2, 2/3, 1). Note - $K_\gamma = 2F_\gamma$.

ϕ	Passive F_γ									
	$R = 0$		$R = 1/3$		$R = 1/2$		$R = 2/3$		$R = 1$	
	LB	*UB*	*LB*	*UB*	*LB*	*UB*	*LB*	*UB*	*LB*	*UB*
0	0.500	0.500	0.500	0.500	0.500	0.500	0.500	0.500	0.500	0.500
1	0.518	0.518	0.521	0.521	0.522	0.522	0.523	0.523	0.524	0.524
2	0.536	0.537	0.542	0.542	0.544	0.545	0.546	0.547	0.549	0.550
3	0.555	0.556	0.564	0.565	0.568	0.569	0.571	0.572	0.576	0.577
4	0.575	0.576	0.588	0.589	0.593	0.594	0.598	0.599	0.604	0.606
5	0.596	0.597	0.612	0.614	0.619	0.621	0.626	0.627	0.634	0.636
6	0.617	0.618	0.638	0.640	0.647	0.649	0.655	0.657	0.666	0.668
7	0.639	0.641	0.665	0.667	0.677	0.679	0.686	0.688	0.700	0.703
8	0.662	0.664	0.694	0.696	0.707	0.710	0.719	0.722	0.736	0.739
9	0.688	0.686	0.726	0.724	0.743	0.740	0.757	0.754	0.778	0.774
10	0.710	0.713	0.755	0.758	0.774	0.778	0.791	0.795	0.815	0.820
11	0.736	0.739	0.788	0.792	0.811	0.815	0.831	0.835	0.858	0.865
12	0.763	0.766	0.823	0.827	0.849	0.854	0.873	0.877	0.905	0.912
13	0.790	0.794	0.860	0.864	0.890	0.896	0.917	0.923	0.955	0.963
14	0.819	0.824	0.899	0.904	0.934	0.940	0.965	0.972	1.008	1.018
15	0.849	0.854	0.940	0.945	0.980	0.987	1.015	1.023	1.065	1.077
16	0.881	0.886	0.983	0.990	1.029	1.036	1.070	1.077	1.126	1.139
17	0.913	0.919	1.029	1.036	1.081	1.089	1.127	1.136	1.193	1.208
18	0.947	0.954	1.077	1.086	1.136	1.146	1.189	1.199	1.264	1.281
19	0.983	0.990	1.129	1.137	1.196	1.207	1.256	1.268	1.340	1.360
20	1.020	1.028	1.184	1.192	1.259	1.270	1.328	1.340	1.428	1.448
21	1.059	1.067	1.242	1.251	1.327	1.341	1.404	1.421	1.514	1.541
22	1.099	1.109	1.304	1.317	1.400	1.415	1.487	1.506	1.611	1.640
23	1.142	1.152	1.370	1.383	1.480	1.495	1.577	1.595	1.724	1.753
24	1.186	1.198	1.440	1.455	1.561	1.578	1.674	1.696	1.831	1.872
25	1.232	1.245	1.515	1.529	1.651	1.670	1.779	1.801	1.956	2.002
26	1.281	1.294	1.594	1.613	1.748	1.772	1.894	1.919	2.096	2.146
27	1.332	1.346	1.681	1.702	1.851	1.880	2.016	2.046	2.244	2.306
28	1.385	1.400	1.773	1.791	1.968	1.994	2.152	2.186	2.406	2.482
29	1.441	1.456	1.871	1.892	2.088	2.118	2.298	2.338	2.586	2.672
30	1.500	1.517	1.976	2.002	2.224	2.256	2.460	2.504	2.800	2.882
31	1.562	1.581	2.092	2.124	2.370	2.404	2.636	2.682	3.016	3.118
32	1.627	1.649	2.214	2.246	2.528	2.568	2.830	2.882	3.258	3.390
33	1.696	1.718	2.348	2.382	2.702	2.744	3.046	3.106	3.524	3.682
34	1.769	1.795	2.492	2.536	2.888	2.948	3.282	3.352	3.842	4.000
35	1.845	1.869	2.648	2.692	3.096	3.158	3.536	3.628	4.180	4.370
36	1.926	1.956	2.806	2.868	3.330	3.402	3.834	3.938	4.564	4.814
37	2.012	2.046	3.004	3.070	3.578	3.666	4.156	4.270	4.978	5.266
38	2.102	2.130	3.204	3.270	3.856	3.940	4.518	4.654	5.456	5.812
39	2.198	2.232	3.432	3.508	4.168	4.266	4.928	5.098	5.992	6.456
40	2.300	2.334	3.670	3.746	4.502	4.626	5.396	5.584	6.632	7.130

6. Comparison and Examples

6.1. Example 1: Cohesionless Soil (Sand, Passive)

A vertical retaining wall, 5 m high with roughness ($R = 0.5$), retains a backfill sand ($c = 0$ kPa,$\phi = 30$). The surface is level with the top of the wall. The unit weight of the sand (γ) is 18 kN/m^3. Determine the passive earth pressure without considering the surcharge pressure ($\sigma_s = 0$).

- For $R = 1/2$ and $\phi = 30°$, Table 6 gives passive $(F_\gamma)_{LB} = 2.224$ and $(F_\gamma)_{UB} = 2.256$.
- Since ($\sigma_s = 0$) and ($c = 0$), equation (4) reduces to $P_P = \gamma H^2 F_\gamma$. The total passive thrust can be calculated as: $(P_p)_{LB} = 1000.8$ kN/m and $(P_p)_{UB} = 1015.2$ kN/m. It is important to note the "missing 1/2" in $P_P = \gamma H^2 F_\gamma$. To compare our ($F_\gamma$) values with those published K_γ values, our F_γ results must be times by two.
- Table 7 compares the results with those from other available methods. Both Terzaghi and Pecks' results and Zhu and Qians' results are close to ours using the stability factors.

6.2. Example 2: Undrained Clay (Active)

A smooth ($R = 0$) vertical retaining wall, 4 m high, retains a horizontal backfill of undrained clay (ϕ=0°) with a unit weight (γ) of 17 kN/m^3. The internal friction angle $\phi = 0°$. The cohesion (c) is chosen to be (10) to (50) kPa. Determine the total active thrust against the wall using the stability factor method and Rankine's method. Consider the surcharge is zero ($\sigma_s = 0$).

- For $R = 0$ and$\phi = 0°$, Tables 1 and 3 give $(F_c)_{LB} = (F_c)_{UB} = 2.001$, $(F_\gamma)_{LB} = (F_\gamma)_{UB} = 0.500$.
- It is important to note the "missing 1/2" in $P_P = \gamma H^2 F_\gamma$. To compare our ($F_\gamma$) values with those published K_γ values, our F_γ results must be times by two.
- Since ($\sigma_s = 0$), equation 3 reduces to $P_A = -cF_cH + \gamma H^2 F_\gamma$.
- Table 8 compares the total active thrusts with Rankin's solution for a smooth wall for $c = 0$, 10, 20, 30, 40, 50 kPa. In general, the current solutions agree well with Rankine's. Since UB = LB for this smooth Rankine wall, Table 8 shows that both the active thrusts are the same, i.e., the exact solution for the Rankine wall.

6.3. Example 3: Cohesive-Frictional soil (Passive)

A smooth ($R = 0$) vertical retaining wall, 5 m high, retains a horizontal backfill of c-ϕ soil. The angle of soil internal friction (ϕ) is 30°, the cohesion (c) is 35 kPa, and the unit weight (γ) is 19 kN/m^3. Determine the total passive thrust using the stability factor method and Rankine's method considering the surcharge is zero ($\sigma_s = 0$).

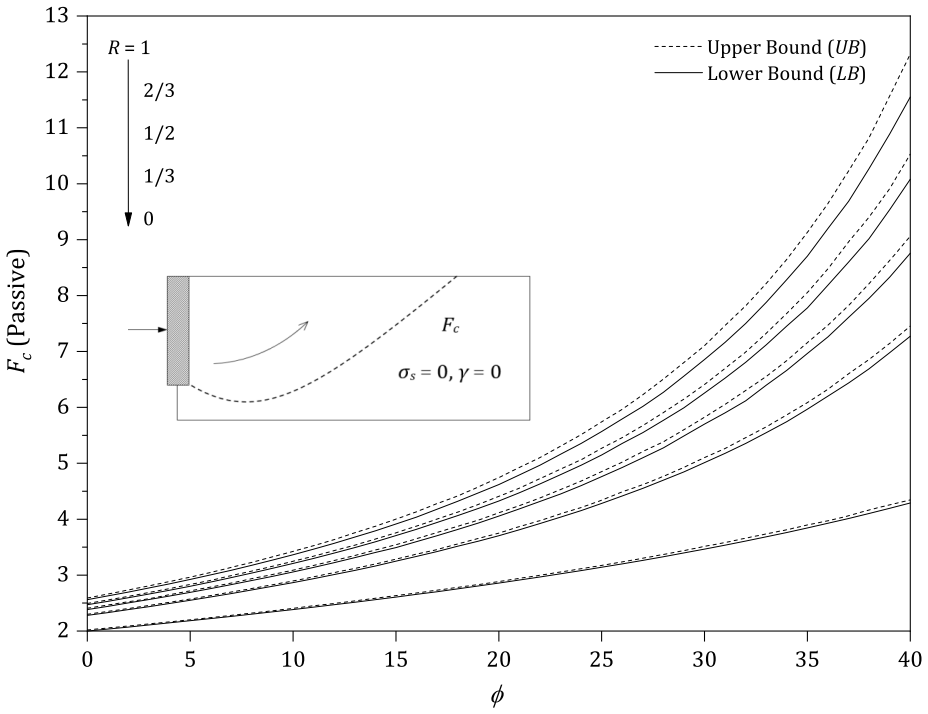

Fig. 7. Passive F_c vs ϕ for various wall roughness.

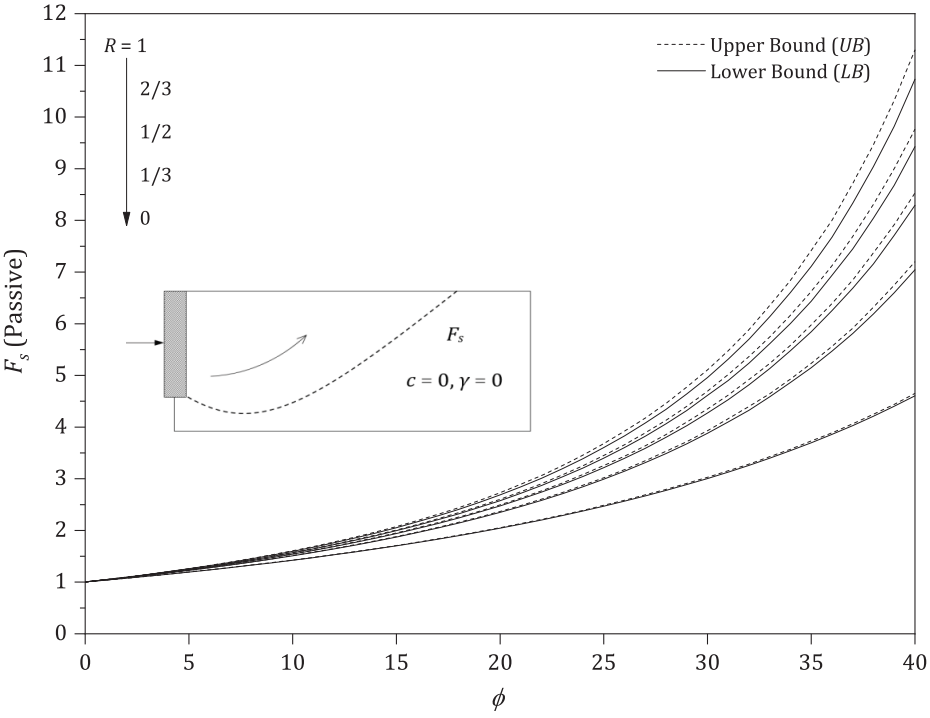

Fig. 8. Passive F_s vs ϕ for various wall roughness.

- For $R = 0$ and $\phi = 30^{\circ}$, Tables 4 - 6 give $(F_c)_{LB} = 3.466$ and $(F_\gamma)_{LB} = 1.500$.
- For $R = 0$ and $\phi = 30^{\circ}$, Tables 4 - 6 give $(F_c)_{UB} = 3.514$ and $(F_\gamma)_{UB} = 1.517$.
- It is important to note the "missing 1/2" in $P_P = \gamma H^2 F_\gamma$. To compare our (F_γ) values with those published K_γ values, our F_γ results must be times by two.
- The total passive thrusts can be calculated from equation (4). $(P_p)_{LB} = 1319.15$ kPa and $(P_p)_{UB} = 1335.72$ kPa.
- Using Rankine's method, for $\phi = 30^{\circ}$, the passive earth pressure coefficient, $K_p = 3.0$. The equation, $P_P = \frac{1}{2} K_P \gamma H^2 + 2c\sqrt{K_p}\, H$, gives a total passive thrust $P_P = 1318.72$ kPa.
- Rankine's solution, which is a stress-based method, is close to our stress-based lower bound solution.

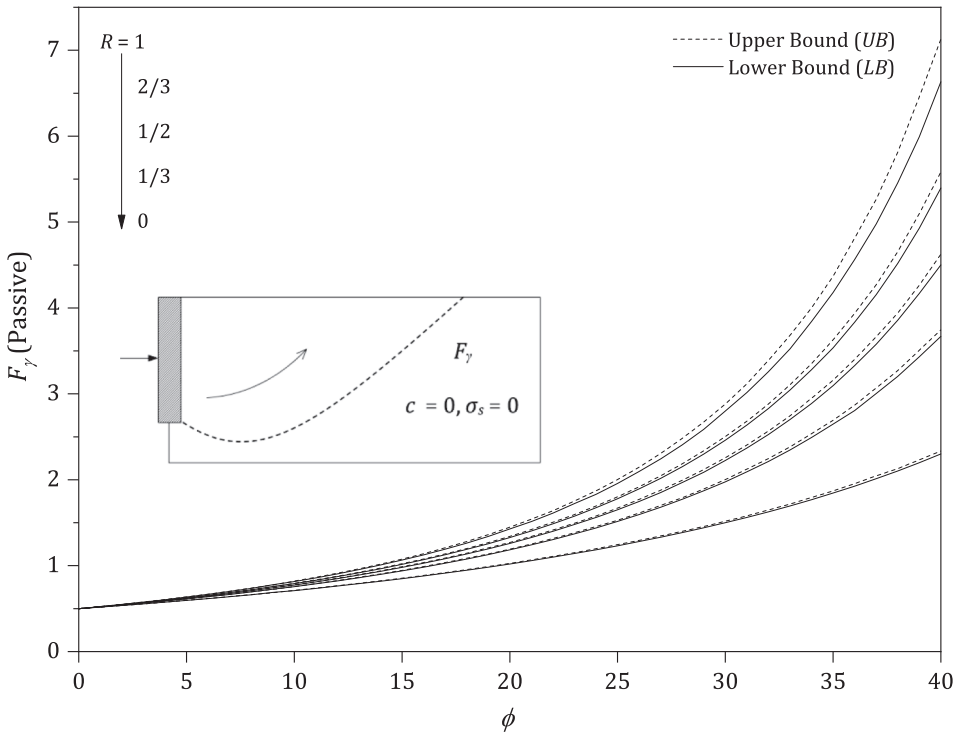

Fig. 9. Passive F_γ vs ϕ for various wall roughness.

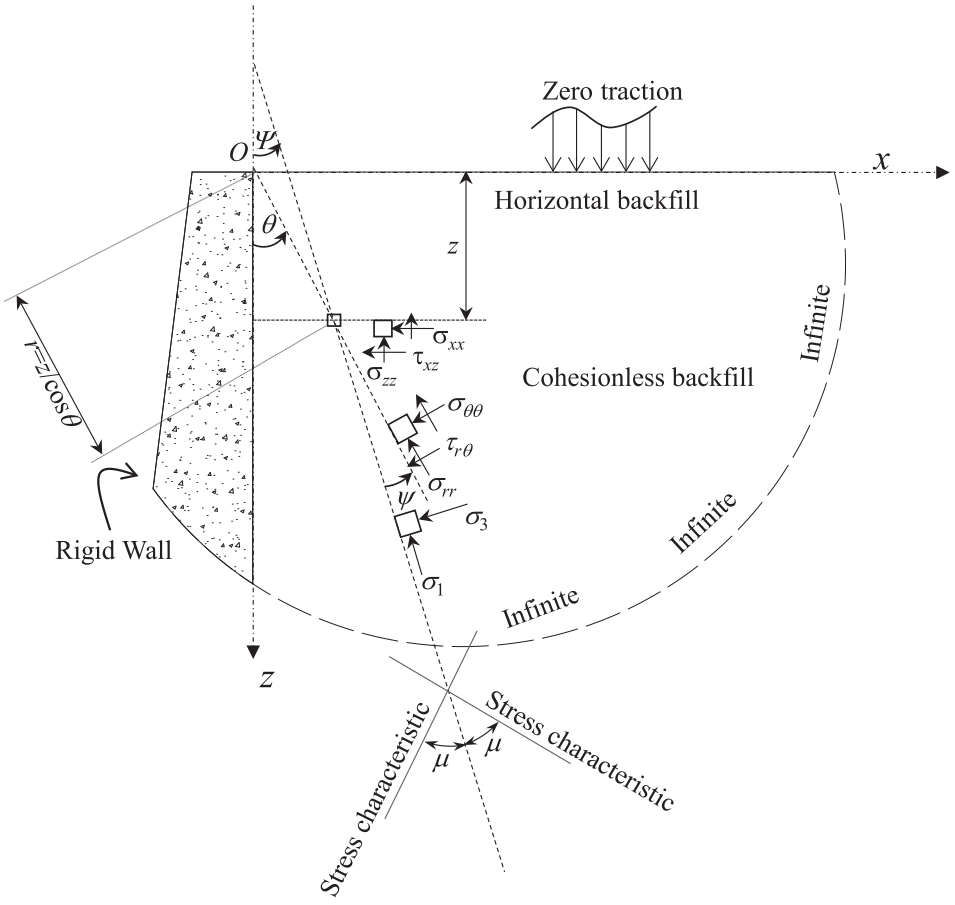

Fig. 10. Geometries of retaining walls with various backfill geometries together with stress components along various planes.

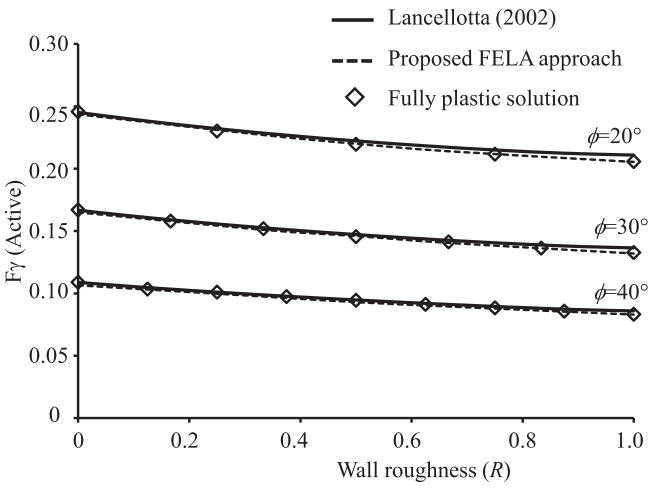

Fig. 11. Comparison of F_γ value for active earth pressures between the proposed FELA approach, fully plastic solution, and Lancellotta's (2002) analytical solution.

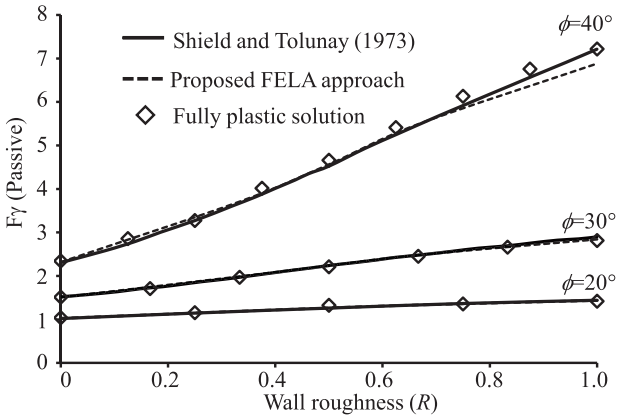

Fig. 12. Comparison of F_γ value for passive earth pressures between the proposed FELA approach, fully plastic solution, and Log-spiral solution solved by Shields and Tolunay (1973).

6.4. Example 4: Surcharge (σ_s, active)

Consider a 5.5 m high (H) retaining wall (smooth, $R = 0$) with a vertical back and a horizontal backfill soil with properties ($c = 0$) and (ϕ=34°). The unit weight of soil (γ) is 18 kN/m^3. Calculate the total active thrust acting on the wall using the stability factor method and the Rankine's method, assuming the range of surcharge pressures ($\sigma_s = 0$ to 40 kPa).

- For $R = 0$ and $\phi = 34°$, Tables 2 and 3 give $(F_s)_{LB} = 0.281$ and $(F_\gamma)_{LB} = 0.141$.
- For $R = 0$ and $\phi = 34°$, Tables 2 and 3 give $(F_s)_{UB} = 0.278$ and $(F_\gamma)_{UB} = 0.139$.
- Equation 3 reduces to $P_A = \gamma H^2 F_\gamma$ with ($c = 0$) and ($\sigma_s = 0$), and the total active thrust $(P_A)_{LB} = 76.77$ kN/m and $(P_A)_{UB} = 75.69$ kN/m.
- It is important to note the "missing 1/2" in $P_P = \gamma H^2 F_\gamma$. To compare our ($F_\gamma$) values with those published K_γ values, our F_γ results must be times by two.
- Please note that for the active stability problems, $(P_A)_{LB} > (P_A)_{UB}$. This is unlike most passive stability problems, in which upper bound results are always higher than lower bound ones.
- With non-zero surcharge $\sigma_s \neq 0$, $P_A = \sigma_s F_s H + \gamma H^2 F_\gamma$ should be used. Table 9 shows the total active thrusts for the various surcharges σ_s = 0, 10, 20, 30, and 40 kPa.
- The results are also compared with other available solutions in Table 9. Overall, good agreement is found amongst the methods.

6.5. Example 5: Wall Roughness (R, Passive)

Consider a 4.5 m high (H) retaining wall with a vertical back and a horizontal granular backfill soil ($c = 0$ kPa, ϕ= 30). The surcharge, σ_s is zero and the unit weight of soil (γ) is 16 kN/m^3. Determine the total passive thrust for wall roughness (R = 0, 1/3, 1/2, 2/3, and 1).

- Since ($\sigma_s = 0$) and ($c = 0$), equation (4) reduces to $P_P = \gamma H^2 F_\gamma$.
- For $R = 0$ and $\phi = 30°$, Table 6 gives passive $(F_\gamma)_{LB} = 1.500$ and $(F_\gamma)_{UB} = 1.517$. The total passive thrust can be calculated as: $(P_p)_{LB} = 486.06$ kN/m and $(P_p)_{UB} = 491.64$ kN/m.
- It is important to note the "missing 1/2" in $P_P = \gamma H^2 F_\gamma$. To compare our ($F_\gamma$) values with those published K_γ values, our F_γ results must be times by two.
- Repeat the same process for (R = 1/3, 1/2, 2/3, and 1), and the results are presented in Table 10 with other available solutions.
- It was found that both Terzaghi and Pecks' results and Zhu and Qians' results are close to our solutions using the stability factors.

7. Conclusion

Similar to the traditional bearing capacity equation of Terzaghi, two new equations, $P_A = -cF_cH + \sigma_s F_s H + \gamma H^2 F_\gamma$ and $P_P = cF_cH + \sigma_s F_s H + \gamma H^2 F_\gamma$ were introduced to determine the total active and passive earth thrusts using the three rigorous stability factors (F_c, F_s, and F_γ), which are functions of both the friction angle of soil ϕ and the wall roughness (R).

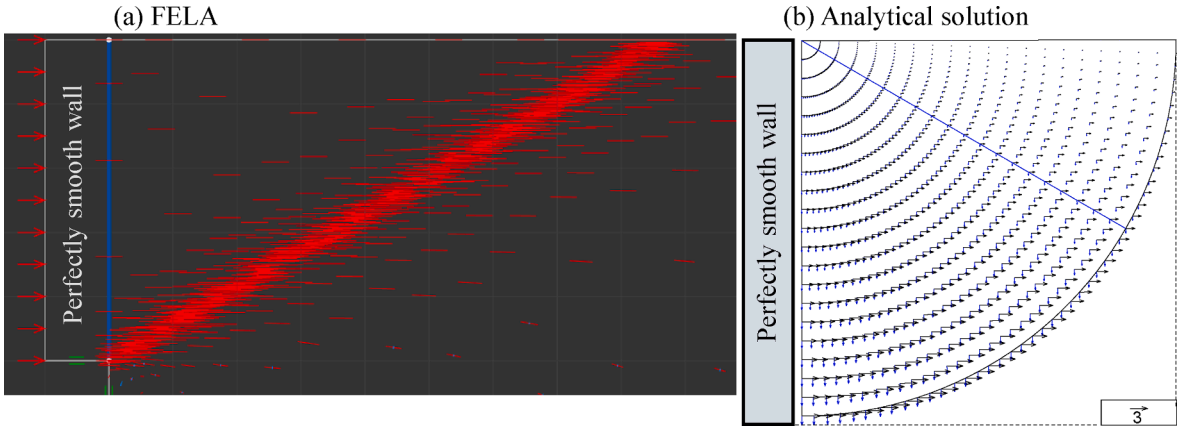

Fig. 13. Trajectories of principal stresses in cohesionless backfill of behind a perfectly smooth wall (φ = 40°) under passive earth pressure using (a) FELA, (b) the analytical lower-bound type solution.

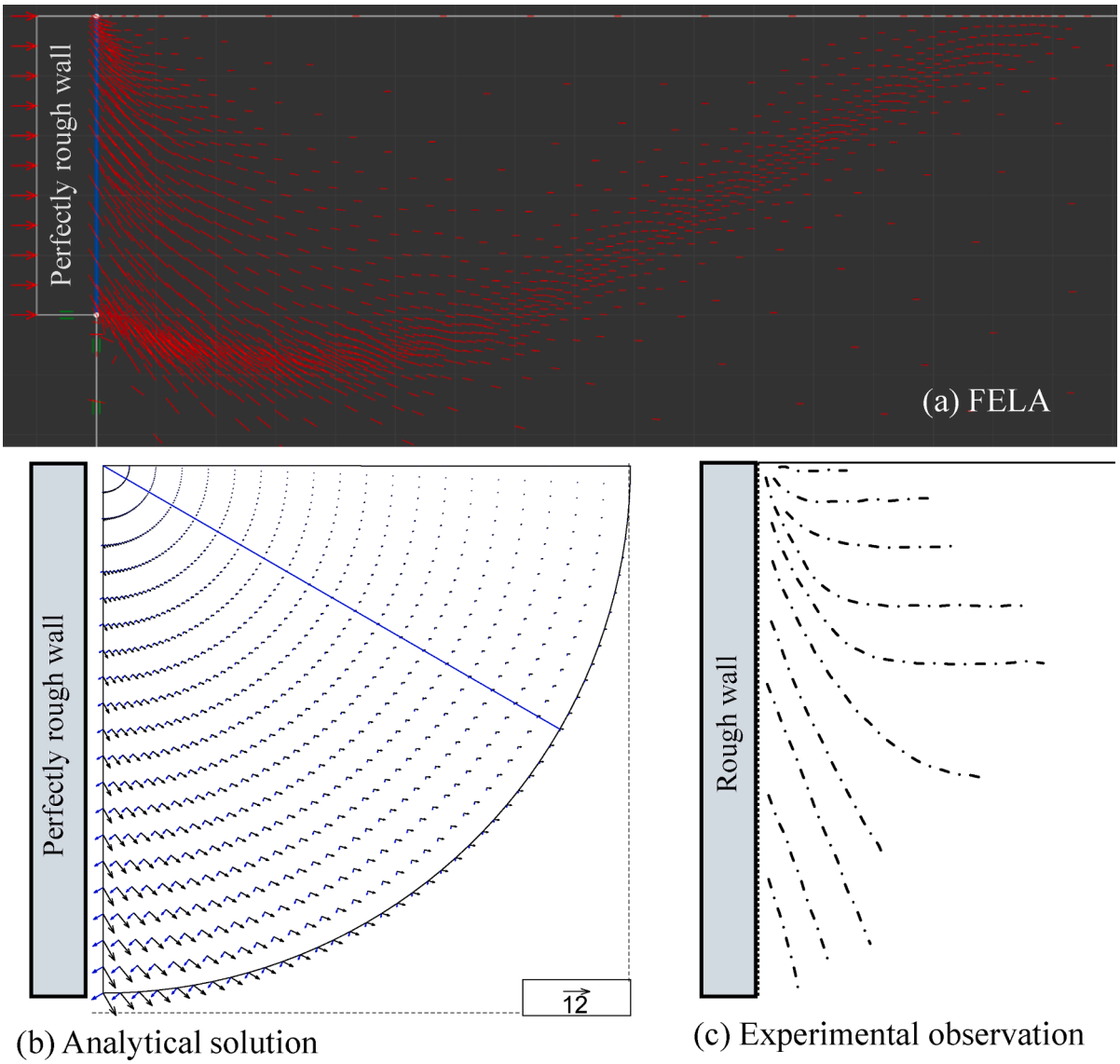

Fig. 14. Trajectories of principal stresses in cohesionless backfill of behind a perfectly rough wall under passive earth pressure (φ = 40°) using (a) FELA, (b) the analytical solution, (c) Experimental observation on principal compressive strength increment trajectories conducted by James and Bransby (1970).

Table 7
Comparison in Example 1 (Das and Sobhan, 2013).

Methods	Passive earth pressure coefficient, K_p	Total passive thrust, P_p (kN/m)
Coulomb's method	4.977	1119.83
Terzaghi and Peck's wedge theory	4.600	1035.00
Shields and Tolunay's solution (method of slices)	4.130	929.25
Zhu and Qian's solution (method of triangular slices)	4.575	1029.38
Caquot and Kerisel's theory	4.774	1074.15
This paper (Stability Factors, *UB*)	4.575	1015.20
This paper (Stability Factors, *LB*)	4.774	1000.80

Table 8
Comparison in Example 2.

Cohesion, c (kPa)	Total active thrust, P_A (kN/m)		
	Rankine Method	This paper (*LB**)	This paper (*UB**)
10	56	55.96	55.96
20	−24	−24.08	−24.08
30	−104	−104.12	−104.12
40	−184	−184.16	−184.16
50	−264	− 264. 20	−264. 20

* Since UB = LB for this smooth Rankine wall, Table 8 shows that both the active thrusts are the same, i.e., the exact solution for the Rankine wall.

Upper and lower bound finite element limit analyses (FELA) were adopted as numerical tools to obtain (F_c, F_s, and F_γ) for a wide range of internal friction angles of backfill soil ($\phi = 0^\circ - 40$) and wall roughness ($R = 0, 1/3, 1/2, 2/3, 1$).

Several conservative solutions based on analytical statically admissible stress fields were successfully adopted to validate the proposed FELA holistic solution, and good agreements were achieved from the comparisons convince the accuracy and reliability of the proposed approach. Furthermore, the effect of the wall's roughness on the load transfer mechanism in cohesionless backfills has been revealed by the proposed approach. The presence of wall roughness potentially rotates the direction of the major principal stress which has been concurrently observed in FELA results, analytical lower-bound type solution (Nguyen

Table 9
Comparison in Example 4 (Das and Sobhan, 2013).

Surcharge, σ_s (kN/m^2)	Total active thrust, P_A (kN/m)			
	Rankine's method	Coulomb's method	This paper (*LB**)	This paper (*UB**)
0	76.97	76.97	76.77	75.69
10	92.52	92.51	92.22	90.98
20	108.07	108.06	107.68	106.27
30	123.62	123.61	123.14	121.56
40	139.17	139.16	138.59	136.85

* Note that for the active stability problems, $(P_A)_{LB} > (P_A)_{UB}$. This is unlike most passive stability problem, in which upper bound results are always higher than lower bound ones.

Table 10
Comparison in Example 5 (Das and Sobhan, 2013).

R	Total passive thrust, P_p (kN/m)						
	Coulomb's method	Terzaghi and Peck's wedge theory	Shields and Tolunay's solution	Zhu and Qian's solution	Caquot and Kerisel's theory	This paper (*LB*)	This paper (*UB*)
0	486.00	486.00	486.00	486.00	484.22	486.06	491.64
1/3	671.17	664.20	615.60	648.00	670.52	640.29	648.65
1/2	806.27	745.20	669.06	741.15	773.39	720.58	730.94
2/3	989.01	842.40	712.80	850.50	887.11	797.04	811.30
1	–	1053.0	842.40	1069.20	1036.80	907.20	933.77

2022), and experimental approach (James and Bransby 1970). The results obtained from the proposed solution exhibit a remarkable level of agreement with those acquired through both analytical and experimental approaches, pertaining to the characteristics of load transfer mechanisms within the backfill. This unequivocally demonstrates the FELA's exceptional versatility and efficacy in addressing lateral earth pressure problems.

This study establishes a quantitative framework of stability factors approach that can be used to determine both active and passive earth pressures with various backfill soil types (cohesionless, cohesive, or cohesive-frictional soils), wall roughness (0, 1/3, 1/2, 2/3, 1), and surcharge pressures. Design tables, charts were developed for practical uses. Five examples were presented to demonstrate the uses of these rigorous factors to estimate earth thrusts on retaining walls. The current study contributes in several ways to our understanding of using stability factors to determine limit loads. Further research may include the backfill inclination as well as to machine learning the comprehensive datasets for practical uses. The effect of unsaturated backfills and soil anisotropy shall also be studied.

CRediT authorship contribution statement

Tan Nguyen: Conceptualization, Methodology, Software, Validation, Formal analysis, Investigation, Resources, Data curation, Writing – original draft, Writing – review & editing, Visualization. **Jim Shiau:** Conceptualization, Methodology, Software, Validation, Formal analysis, Investigation, Resources, Data curation, Writing – original draft, Writing – review & editing, Visualization, Supervision, Project administration.

Declaration of Competing Interest

The authors declare that they have no known competing financial interests or personal relationships that could have appeared to influence the work reported in this paper.

Data availability

Data will be made available on request.

References

Antao, N., Santana, G., Silva, D.a., Guerra, N.M.D.C., 2011. Passive earth-pressure coefficients by upper-bound numerical limit analysis. Can. Geotech. J. 48 (5), 767–780.

Antao, N., Santana, G., Silva, D., Guerra, N.M.C., 2016. Three-dimensional active earth pressure coefficients by upper bound numerical limit analysis. Comput. Geotech. 79, 96–104.

Basudhar, P.K., Madhav, R., 1980. Simplified passive earth pressure analysis. J. Geotech. Eng. Div. 106 (4), 470–474.

Bellezza, I., 2014. A new pseudo-dynamic approach for seismic active soil thrust. Geotech. Geol. Eng. 32 (2), 561–576. https://doi.org/10.1007/s10706-014-9734-y.

Benmeddour, D., Mellas, M., Frank, R., Mabrouki, A., 2012. Numerical study of passive and active earth pressures of sands. Comput. Geotech. 40, 34–44.

Caquot, A. & Kerisel, 1948, Tables for the calculation of passive pressure, active pressure and bearing capacity of foundations, Gautier-Villars, Paris.

Chang, M.-F., 1997. Lateral earth pressures behind rotating walls. Can. Geotech. J. 34 (4), 498–509.

Chen, W.F., Rosenfarb, J.L., 1973. Limit analysis solutions of earth pressure problems. Soils Found. 13 (4), 45–60.

Choudhury, D., Nimbalkar, S., 2005. Seismic passive resistance by pseudo-dynamic method. Géotechnique 55 (9), 699–702. https://doi.org/10.1680/geot.2005.55.9.699.

Das, BM & Sobhan, K 2013, 'Lateral Earth Pressure: Curved Failure Surface', in Principles of Geotechnical Engineering, 8th edn.

Duncan, J., Mokwa, L., 2001. Passive earth pressures: Theories and tests. J. Geotech. Geoenviron. Eng. 127 (3), 248–257.

Fang, Y.-S., Ishibash, I., 1986. Static earth pressures with various wall movements. J. Geotech. Eng. 112 (3), 317–333.

Fathipour, H., Payan, M., Jamshidi Chenari, R., Senetakis, K., 2021a. Lower bound analysis of modified pseudo-dynamic lateral earth pressures for retaining wall-backfill system with depth-varying damping using FEM-Second order cone programming. Int. J. Numer. Anal. Meth. Geomech. 45 (16), 2371–2387. https://doi.org/10.1002/nag.3269.

Fathipour, H., Siahmazgi, A.S., Payan, M., Veiskarami, M., Jamshidi Chenari, R., 2021b. Limit analysis of modified pseudodynamic lateral earth pressure in anisotropic frictional medium using finite-element and second-order cone programming. Int. J. Geomech. 21 (2) https://doi.org/10.1061/(asce)gm.1943-5622.0001924.

Fathipour, H., Safardoost Siahmazgi, A., Payan, M., Jamshidi Chenari, R., Veiskarami, M., 2023. Evaluation of the active and passive pseudo-dynamic earth pressures using finite element limit analysis and second-order cone programming. Geotech. Geol. Eng. 41 (3), 1921–1936. https://doi.org/10.1007/s10706-023-02381-0.

Iskandern, M., Chen, Z., Omidvar, M., Guzman, I., Elsherif, O., 2013. Active static and seismic earth pressure for c–φ soils. Soils Found. 53 (5), 639–652.

James, R.G., Bransby, P.L., 1970. Experimental and theoretical investigations of a passive earth pressure problem. Géotechnique 20 (1), 17–37. https://doi.org/10.1680/geot.1970.20.1.17.

Keawsawasvong, S., Ukritchon, B., 2019. Undrained stability of a spherical cavity in cohesive soils using finite element limit analysis. J. Rock Mech. Geotech. Eng. 11 (6), 1274–1285.

Krabbenhoft, K., 2018. Static and seismic earth pressure coefficients for vertical walls withhorizontal backfill. Soil Dyn. Earthq. Eng. 104, 403–407.
Krabbenhoft, K., 2019. "Plastic design of embedded retaining walls". Proceedings of the Institution of Civil Engineers - Geotechnical Engineering 172 (2), 131–144.
Kumar, J., Chitikela, S., 2002. Seismic passive earth pressure coefficients using the method of characteristics. Can. Geotech. J. 39 (2), 463–471.
Lancellotta, R., 2002. Analytical solution of passive earth pressure. Géotechnique 52 (8), 617–619. https://doi.org/10.1680/geot.2002.52.8.617.
Li, Z.-W., Yang, X.-L., 2023. Pseudodynamic estimation of 3D active earth pressures with a nonlinear strength criterion. Int. J. Geomech. 23 (8) https://doi.org/10.1061/ijgnai.gmeng-7667.
Liu, X., Ou, M., Yang, X., 2013. Upper bound limit analysis of passive earth pressure of cohesive backfill on retaining wall. Appl. Mech. Mater. 353–356, 895–900.
Liu, S., Xia, Y., Liang, L., 2018. A modified logarithmic spiral method for determining passive earth pressure. J. Rock Mech. Geotech. Eng. 10 (6), 1171–1182. https://doi.org/10.1016/j.jrmge.2018.03.011.
Mirmoazen, S.M., Lajevardi, S.H., Mirhosseini, S.M., Payan, M., Jamshidi Chenari, R., 2021a. Limit analysis of lateral earth pressure on geosynthetic-reinforced retaining structures subjected to strip footing loading using finite element and second-order cone programming iranian journal of science and technology. Transactions of Civil Engineering 46 (4), 3181–3192. https://doi.org/10.1007/s40996-021-00793-7.
Mirmoazen, S.M., Lajevardi, S.H., Mirhosseini, S.M., Payan, M., Chenari, R.J., 2021b. Active lateral earth pressure of geosynthetic-reinforced retaining walls with inherently anisotropic frictional backfills subjected to strip footing loading. Comput. Geotech. 137, 104302. https://doi.org/10.1016/j.compgeo.2021.104302.
Nguyen, T., 2022. Passive earth pressures with sloping backfill based on a statically admissible stress field. Comput. Geotech. 149, 104857. https://doi.org/10.1016/j.compgeo.2022.104857.
Nguyen, T., 2023a. An exact solution of active earth pressures based on a statically admissible stress field. Comput. Geotech. 153, 105066. https://doi.org/10.1016/j.compgeo.2022.105066.
Nguyen, T., 2023b. Statically admissible stress fields in conical sand valleys and heaps: A validation of haar–von kármán hypothesis. Int. J. Geomech. 23 (2) https://doi.org/10.1061/ijgnai.gmeng-7863.
Nguyen, T., Pipatpongsa, T., 2020. Plastic behaviors of asymmetric prismatic sand heaps on the verge of failure. Mech. Mater. 151, 103624. https://doi.org/10.1016/j.mechmat.2020.103624.
O'Neal, S., Hagerty, D.J., 2011. Earth pressures in confined cohesionless backfill against tall rigid walls - a case history. Can. Geotech. J. 48 (8), 1188–1197.
OptumCE 2020, OptumG2. Copenhagen, Denmark: Optum Computational Engineering. See https://optumce.com/.
Patki, M.A., Dewaikar, D.M., Mandal, J.N., 2017. Numerical evaluation of passive earth-pressure coefficients under the effect of surcharge loading. Int. J. Geomech. 17 (3), 06016024.
Pufahl, D.E., Fredlund, D.G., Rahardjo, H., 1983. Lateral earth pressures in expansive clay soils. Can. Geotech. J. 20 (2), 228–241. https://doi.org/10.1139/t83-027.
Shiau, J., Al-Asadi, F., 2020a. Determination of critical tunnel heading pressures using stability factors. Comput. Geotech. 119, 103345.
Shiau, J., Al-Asadi, F., 2020b. Two-dimensional tunnel heading stability factors Fc, Fs and Fγ. Tunn. Undergr. Space Technol. 97, 103293.
Shiau, J., Al-Asadi, F., 2020c. Twin tunnels stability factors Fc, Fs and Fγ. Geotech. Geol. Eng. https://doi.org/10.1007/s10706-020-01495-z.
Shiau, J., Augarde, C.E., Lyamin, A.V., Sloan, S.W., 2008. Finite element limit analysis of passive earth resistance in cohesionless soils. Soils Found. 48 (6), 843–850.
Shiau, J., Lai, V.Q., Keawsawasvong, S., 2022. Multivariate adaptive regression splines analysis for 3D slope stability in anisotropic and heterogenous clay. J. Rock Mech. Geotech. Eng. https://doi.org/10.1016/j.jrmge.2022.05.016.
Shiau, J., Smith, C., 2006. Numerical analysis of passive earth pressures with interfaces. III European Conference on Computational Mechanics. Springer, Dordrecht.
Shiau, J., Lyamin, A.V., Sloan, S.W., 2004. 'Rigorous solution of classical lateral earth pressures', 6th Young Geotechnical Professionals Conference. Gold Coast, Australia, pp. 162–167.
Shiau, J., Lyamin, AV., Sloan, SW., 2006. 'Application of pseudo-static limit analysis in geotechnical earthquake design'. Proceedings of the 6th European Conference on Numerical Methods in Geotechnical Engineering 249–255.
Shields, H., Tolunay, A., 1973. Passive pressure coefficients by method of slices. Journal of the Soil Mechanics and Foundations Division 99 (12), 1043–1053.
Sloan, S.W., 2013. Geotechnical stability analysis. Géotechnique 63 (7), 531–571.
Sokolovski, V., 1960. Statics of soil media (translated from Russian by dh jones and an schofield). Butterworth, London, England 21, 369–395.
Sokolovskii, V.V., 1965. Statics of granular media. Pergamon. 284.
Soubra, AH & Macuh, B 2002, 'Active and passive earth pressure coefficients by a kinematical approach', Proceedings of the Institution of Civil Engineers - Geotechnical Engineering, vol 155 , no. 2, pp. 119-131.
Tang, C., Phoon, K.-K., Toh, K.-C., 2014. Lower-bound limit analysis of seismic passive earth pressure on rigid walls. Int. J. Geomech. 14 (5), 04014022.
Terzaghi, K 1943, Theoretical soil mechanics.
Terzaghi, K & Peck, RB 1967, 'Plastic equilibrium in soils', in Soil Mechanics in Engineering Practice, 3rd edn.
Tsagareli, Z.V., 1965. Experimental investigation of the pressure of a loose medium on retaining walls with a vertical back face and horizontal backfill surface. Soil Mech. Found. Eng. 2 (4), 197–200.
Ukritchon, B., Keawsawasvong, S., 2018. A new design equation for drained stability of conical slopes in cohesive-frictional soils. J. Rock Mech. Geotech. Eng. 10 (2), 358–366.
Vo, T., Russell, A.R., 2014. Slip line theory applied to a retaining wall–unsaturated soil interaction problem. Comput. Geotech. 55, 416–428. https://doi.org/10.1016/j.compgeo.2013.09.010.
Yang, X.L., Chen, H., 2021. Seismic analysis of 3D active earth pressure for unsaturated backfill. Transp. Geotech. 30, 100593. https://doi.org/10.1016/j.trgeo.2021.100593.
Zhang, Z.L., Zhu, J.Q., Yang, X.L., 2023. Three-dimensional active earth pressures for unsaturated backfills with cracks considering steady seepage. Int. J. Geomech. 23 (2) https://doi.org/10.1061/(asce)gm.1943-5622.0002648.
Zhu, D.-Y., Qian, Q., 2000. Determination of passive earth pressure coefficients by the method of triangular slices. Can. Geotech. J. 37 (2), 485–491.